FORMATION FLIGHT OF EARTH SATELLITES ON KAM TORUS USING CLASSICAL ORBITAL ELEMENTS

THESIS

Marissa C. Reabe, Captain, USAF

AFIT-ENY-MS-17-M-285

DEPARTMENT OF THE AIR FORCE
AIR UNIVERSITY

AIR FORCE INSTITUTE OF TECHNOLOGY

Wright-Patterson Air Force Base, Ohio

DISTRIBUTION STATEMENT A.
APPROVED FOR PUBLIC RELEASE; DISTRIBUTION UNLIMITED.

The views expressed in this thesis are those of the author and do not reflect the official policy or position of the United States Air Force, Department of Defense, or the United States Government. This material is declared a work of the United States Government and is not subject to copyright protection in the United States.

AFIT-ENY-MS-17-M-285

FORMATION FLIGHT OF EARTH SATELLITES ON KAM TORUS USING CLASSICAL ORBITAL ELEMENTS

THESIS

Presented to the Faculty

Department of Aeronautics and Astronautics

Graduate School of Engineering and Management

Air Force Institute of Technology

Air University

Air Education and Training Command

In Partial Fulfillment of the Requirements for the

Degree of Master of Science in Systems Engineering

Marissa C. Reabe, BS

Captain, USAF

March 2017

DISTRIBUTION STATEMENT A.APPROVED FOR PUBLIC RELEASE; DISTRIBUTION UNLIMITED.

AFIT-ENY-MS-17-M-285

FORMATION FLIGHT OF EARTH SATELLITES ON KAM TORUS USING CLASSICAL ORBITAL ELEMENTS

Marissa C. Reabe, BS

Captain, USAF

Committee Membership:

Dr. William Wiesel
Chair

Lt Col Kirk Johnson, PhD
Member

Capt Adam Comer, PhD
Member

Abstract

This research uses the KAM theory that has been refined by Wiesel to show that Earth-satellite dynamics can be represented by an integrable Hamiltonian system with a small perturbation, like Earth's geopotential. The satellite will follow a torus in phase space and remain on that KAM torus for all time unless acted on by a non-conservative force. A torus frequency was calculated, in this research, using a truth model in System Tool Kit (STK) and the High Precision Orbit Propagator (HPOP) to develop an accurate ephemeris file listing the Classical Orbital Elements (COE). The frequencies found from the truth model were then used to calculate two delta-v maneuvers to insert a satellite onto a desired KAM torus at a specified position and time. Ultimately, this method could be a practical approach to the wider astronautics community to calculate a more accurate satellite position and time over longer periods when compared to current orbital mechanics methods. The results indicated that this particular scenario of "fixing" a satellite on a desired KAM torus using two delta-v maneuvers is not suitable. The residuals for the first test case were on the order of 10^{-7} or greater causing the satellite to lie on a different torus. The linear least squares method produced rough KAM torus frequencies and it was determined this method is not suitable to determine accurate frequencies.

To my daughter, Melanie, my wish upon a star

Acknowledgments

First, I would like to thank my understanding and selfless husband, Jonathan. Thank you for encouraging me to go for my dreams even when I didn't even believe I could do it. To my daughter, Melanie, for being my inspiration during the long hours of thesis writing. Finally, last but not least, to my advisor, Dr. Wiesel. I am grateful for your guidance and patience. Your knowledge of KAM Tori and orbital dynamics is remarkable and has motivated me throughout this entire project.

Marissa Carol Reabe

Table of Contents

Page

Abstract 3

Acknowledgments 5

Table of Contents 6

List of Figures 8

List of Tables 10

List of Acronyms 11

I. Introduction 12

1.1 Background 12
1.2 Iridium Constellation 13
1.3 GPS Constellation 14
1.4 Galileo Constellation 16
1.5 Motivation 17
1.6 Approach 19
1.7 Problem Statement 20
1.8 Investigative Questions 20
1.9 Results 21

II. Background 22

2.1 Chapter Overview 22
2.2 Reference Frames 22
2.3 Newton's Three Laws of Motion 24
2.4 Satellite Orbit Determination 25
2.5 Two-Body Problem 25
2.6 Classic Orbital Elements 28
2.7 Major Perturbations on Earth-orbit satellites 32
2.8 Earth's Geopotential 33
2.9 Orbital Maneuvers 35
2.10 Rocket Equation 36
2.11 Hamiltonian Dynamics 37
2.12 Canonical Transformations and Generating Functions 39
2.13 Hamiltonian-Jacobi Theory 42
2.14 Action-Angle Variables 44
2.15 KAM Theory 47
2.16 Previous Research of KAM Torus 50

III. Methodology 54

3.1 Chapter Overview 54
3.2 Generating Orbital Data for Analysis 54
3.3 Frequency Calculation 56
3.4 State Vector Definition 57
3.5 New Torus Definition 58
3.6 Two Impulse Maneuver Strategy 59
3.7 Canonical Units 63
3.8 New Position and Velocity determination 63
3.9 New Frequency Calculation and Error Residuals 64

IV. Results 65

4.1 Chapter Overview 65
4.2 First Test Case (1 week initial propagation) 65
4.2.1. Initial Frequency Calculations 66
4.2.2. New KAM torus frequency 69
4.2.3. The Two Impulse Maneuver Data 69
4.2.4. New Frequency Calculations 70
4.3 Second Test Case (2 week initial propagation time) 75
4.3.1. Initial Frequency Calculations (Test Case 2) 76
4.3.2. New KAM torus frequency (Test Case 2) 79
4.3.3. The Two Impulse Maneuver Data 79
4.4 Investigative Questions Answered 81

V. Conclusions and Recommendations 83

5.1 Chapter Overview 83
5.2 Conclusions of Research 83
5.3 Significance of Research 84
5.4 Recommendations for Future Research 84
5.5 Summary 85

Bibliography 87

List of Figures

Page
Figure 1: Iridium Constellation [6] 14
Figure 2: Expandable GPS 24-slot satellite constellation [9] 15
Figure 3: Galileo Constellation [10] 16
Figure 4: Satellite Growth Chart [1] 18
Figure 5: Two point masses in inertial reference frame [18] 26
Figure 6: Classical Orbital Elements [18] 28
Figure 7: Kepler's Auxiliary Circles [18] 30
Figure 8: Periodic Motion 45
Figure 9: 1-Dimensional Torus [27] 49
Figure 10: Multi-dimensional Torus [27] 49
Figure 11: Satellite Orbiting a Torus [28] 50
Figure 12: Apsidal Frequency vs Inclination in LEO [26] [30] 53
Figure 13: Mean Anomaly Curve Fit 66
Figure 14: Mean Anomaly Residuals Fit 66
Figure 15: Argument of Perigee Curve Fit 67
Figure 16: Argument of Perigee Residuals 67
Figure 17: RAAN Curve Fit 67
Figure 18: RAAN Residuals Fit 68
Figure 19: RAAN Residuals Fit Zoomed in 68
Figure 20: Maneuver Cost Graph Test Case 1 [13] 70
Figure 21: Mean Anomaly Curve Fit after Maneuver 73

Figure 22: Mean Anomaly Residuals after Maneuver 74
Figure 23: RAAN Curve Fit after Maneuver 74
Figure 24: RAAN Residuals after Maneuver 74
Figure 25: Argument of Perigee Curve Fit after Maneuver 75
Figure 26: Argument of Perigee Residuals after Maneuver 75
Figure 27: Mean Anomaly Curve Fit (Test 2) 77
Figure 28: Mean Anomaly Residuals (Test 2) 77
Figure 29: RAAN Curve Fit (Test 2) 77
Figure 30: RAAN Residuals (Test 2) 78
Figure 31: Argument of Perigee Curve Fit (Test 2) 78
Figure 32: Argument of Perigee Residuals (Test 2) 78
Figure 33: Maneuver Cost Graph Test Case 2 [13] 80
Figure 34: Satellite2 First Maneuver 81

List of Tables

Page
Table 1: Reference Frames [3] 23
Table 2: Classical Orbital Elements [19] 29
Table 3: Canonical Transformations [20] 41
Table 4: Canonical Units 63
Table 5: Case 1 Orbital Parameters Test Case 1 65
Table 6: Curve Fit Data 68
Table 7: New KAM Torus Frequencies 69
Table 8: Impulse Maneuver Data 69
Table 9: New Curve Fit Data 71
Table 10: Orbital Parameters 2nd Test Case 76
Table 11: New KAM Torus Frequencies 79
Table 12: Two Impulse Maneuver Data Test 2 80

List of Acronyms

COE	Classical Orbital Elements
DoD	Department of Defense
ECEF	Earth-Centered Earth Fixed
ECI	Earth-Centered Inertial
EGM-96	Earth Gravitation Model - 1996
GEO	Geostationary Equatorial Orbit
GNSS	Global Navigation Satellite System
GPS	Global Positioning System
HPOP	High Precision Orbit Propagator
KAM	Kolmogorov, Arnold, Moser
LEO	Low Earth Orbit
MATLAB	Matrix Laboratory
MEO	Medium Earth Orbit
NASA	National Aeronautics and Space Administration
NGS	National Geodetic Survey
NOTAM	Notice to Airmen
STK	Systems Tool Kit
TLE	Two Line Element Set
RAAN	Right Ascension of the Ascending Node
SGP4	Simplified General Perturbation 4
USSTRATCOM	United States Strategic Command
UTC	Coordinated Universal Time
WGS84	World Geodetic System 1984

FORMATION FLIGHT OF EARTH SATELLITES ON KAM TORUS USING CLASSICAL ORBITAL ELEMENTS

I. Introduction

1.1 Background

The space environment today is “increasingly contested in all orbits” and orbit station keeping is becoming more important for maintaining a spacecraft’s optimal trajectory to ensure maximum mission effectiveness, avoid collisions with debris or other satellites and protect national interests [1]. In 1957, after the launch of Sputnik, there were only two nations, Russia and the United States, competing for a position above Earth’s atmosphere. Today 60 years later there are over 60 nations struggling for a precious slot in the dwindling Earth orbit environment [1]. “I think [China or Russia will] threaten every orbital regime that we operate in. Now we have to figure out how to defend those satellites, and we're going to. Space Command is making its new satellites more maneuverable to evade attack.” – General John Hyten, Commander, United States Strategic Command (USSTRATCOM) [2]. The precision needed for Earth-satellite dynamics is in high demand as not only are government agencies fighting for a position in space but commercial agencies as well are making space more “competitive” [1].

Station keeping is vital to a satellite’s mission because at any given time it will be in an orbit slightly different than the one predicted; and, if left uncorrected, can accumulate over time to thousands of kilometers off the desired position. The second reason station keeping is so important is the numerous environmental forces acting on a spacecraft: Earth’s gravity; atmospheric drag; third body gravity from the Sun, Moon or other planets; solar radiation; magnetic torque; and finally Earth’s oblateness or J_2 affects. These external forces require some

type of orbit maintenance technique like thrusters or actuators. These perturbations can result in differential satellite motion with cyclic components and continuous secular drift that constantly affect its desired position [3].

To counteract these perturbations, periodic corrections to the orbit need to be made which is where orbit station keeping comes in. Attitude actuators correct a spacecraft's orientation when needed to rotate for station keeping or mission accomplishment like taking pictures or downlinking data. Attitude actuators range from passive to active and apply external or internal torques. Passive actuators often control only one axis and act on a loop using small torques to keep the satellite in its desired position. A few examples of passive actuators are: gravity-gradient stabilization, and spin stabilization and dampers. Active actuators like thrusters, magnetic torquers or momentum-control devices are far more accurate and can supply dual spin or 3-axis stability. [3]

Understanding and determining spacecraft attitude for just one spacecraft requires sensors and actuators that can be expensive depending on the types used and the spacecraft mission's desired accuracy. Determining the attitude for constellations and clusters that need to remain on a certain orbit can be a costly task. The following are examples of constellations that need to remain on a specific orbit and require station keeping to keep them on the mission required orbit.

1.2 Iridium Constellation

The Iridium constellation is a unique satellite communication network that delivers voice and data across the world. Iridium encompasses 66 Low Earth Orbit (LEO) cross-linked satellites with six spares in a near circular polar orbit about an altitude of 780 km [4]. The

constellation has six planes with 11 satellites in each plane [4]. Their mission is to provide full Earth coverage at all times which Figure 1 shows. Iridium has sustained cross-linked architecture of its satellite network to allow the satellites to drift and still keep links with neighboring satellites without requiring a lot of fuel consumption for station keeping [4]. Each satellite has about 100 kg of fuel on board for station keeping [4]. By using periodic propulsive burns, Iridium is able to keep its mission altitude and maintain an orbital period of 1.67 hours and an orbit eccentricity of 0.00126 [5]. The in-plane velocity directions maintain between +/- 6 km and the Right Ascension of the Ascending Node (RAAN) angles maintain about +/- 0.08 degrees with respect to the satellite's in-plane neighbor [5]. Orbital terms used in this research like eccentricity and RAAN will be defined in Section 2.6.

Figure 1: Iridium Constellation [6]

1.3 GPS Constellation

Another example is the Global Position System (GPS), which consists of 24 operational satellites with seven stand-by satellites or back-ups (in case one of the main satellites goes down). In June 2011, the GPS constellation was expanded to include three more satellites to supply more coverage to most parts of the world [7]. The GPS satellites maintain Medium

Earth Orbit (MEO) of about 20,200 km due to the mission of the GPS system to keep a certain number of satellites in view. The satellites are arranged into six orbital planes with nominally four space vehicles (SV) per plane at a 55 degree inclination [8] Figure 2 shows. The MEO was chosen to prevent constant station keeping. When a GPS satellite needs to correct its orbit, the satellite goes offline; a difficult and bothersome issue for a system that has a 24 hour user need. Normally, the Federal Aviation Administration issues a NOTAM (Notice to airmen before a GPS outage and with the multi-global navigation satellite system (GNSS) receivers this outage does not have a big effect on the user [8]. A GPS satellite orbits twice per 24 hour period and keeps at least four satellites within view at a time for GPS users. A GPS end user will need four satellites within line of site to be able to determine their position and time from the ranging signals broadcasted from the satellites.

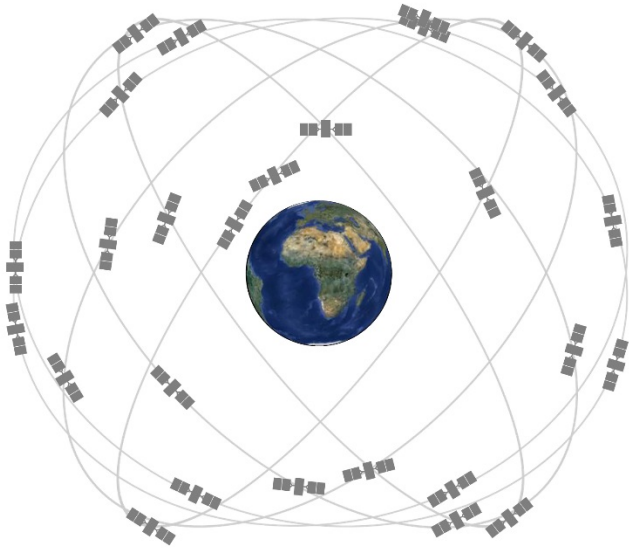

Figure 2: Expandable GPS 24-slot satellite constellation [9]

1.4 Galileo Constellation

The Galileo, European's global satellite navigation network, is currently in production and when fully operational will have 30 satellites in MEO at an altitude of 23,222 km. This constellation design employs 10 satellites per orbital plane with a 56 degree inclination to the equator (a satellite takes about 14 hours to orbit the Earth). There will be two spare satellites on stand-by within each plane. Four satellites are required to determine the end user position and time similar to GPS. Possibly up to eight satellites will be visible from most locations on Earth [10]. Figure 3 shows the Galileo constellation.

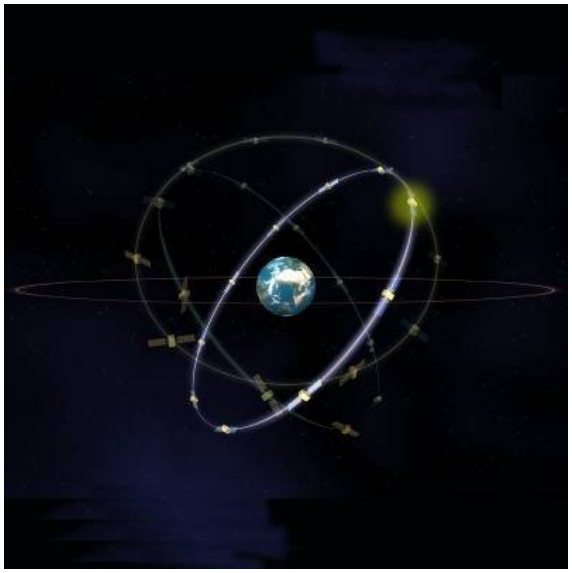

Figure 3: Galileo Constellation [10]

Currently, the Galileo station keeping strategy depends on the user equivalent range error and dilution of position [11]. The goal of station keeping is to keep the "constellation in a configuration that allows ensuring nominal level of service during its whole planned lifetime" [11]. Galileo utilizes propellant for orbit correction maneuvers, which it does so the constellation will not completely lose its geometrical configuration because of the orbital perturbations [11]. Galileo is attempting to keep the following constellation Geometry

Tolerances: RAAN variations less than +/- 2 degrees, inclination variations of less than +/- 2 degrees with along track orbit keeping in the same orbit plane of less than +/- 3 degrees and relative phasing variation between adjacent plans of less than +/- 3 degrees [12]. The number of satellite maneuvers is planned for a maximum of only one per lifetime or 12 years [12].

1.5 Motivation

As can be seen from just three constellation programs, space is becoming increasingly "congested" with the growing global space activity and the increased debris. Station keeping strategies are improving with each new system but there is still a need to correct orientation and continue to monitor constellations in case of collision. Space operations are complicated and expensive for those who want to take advantage of all the opportunities space has to offer [1]. The Department of Defense (DoD) tracks over 22,000 man-made objects in orbit (as seen in Figure 4). With current orbit determination methods, the existing method for approximating celestial and satellite dynamics is an unsolvable problem [1]. Scientists have been searching for a method that will lead to a more practical approach to satellite-Earth dynamics for over 300 years; since the days of Isaac Newton.

Orbit station keeping and understanding the relative motion between two or more satellites orbiting about a primary body is vital to satellite technology applications today. As the employment of satellites increases for companies like Space X and Virgin Galactic, and for government agencies like the European Space Agency, development of satellite formation performance will be the focus for not only commercial and scientific purposes, but also military applications.

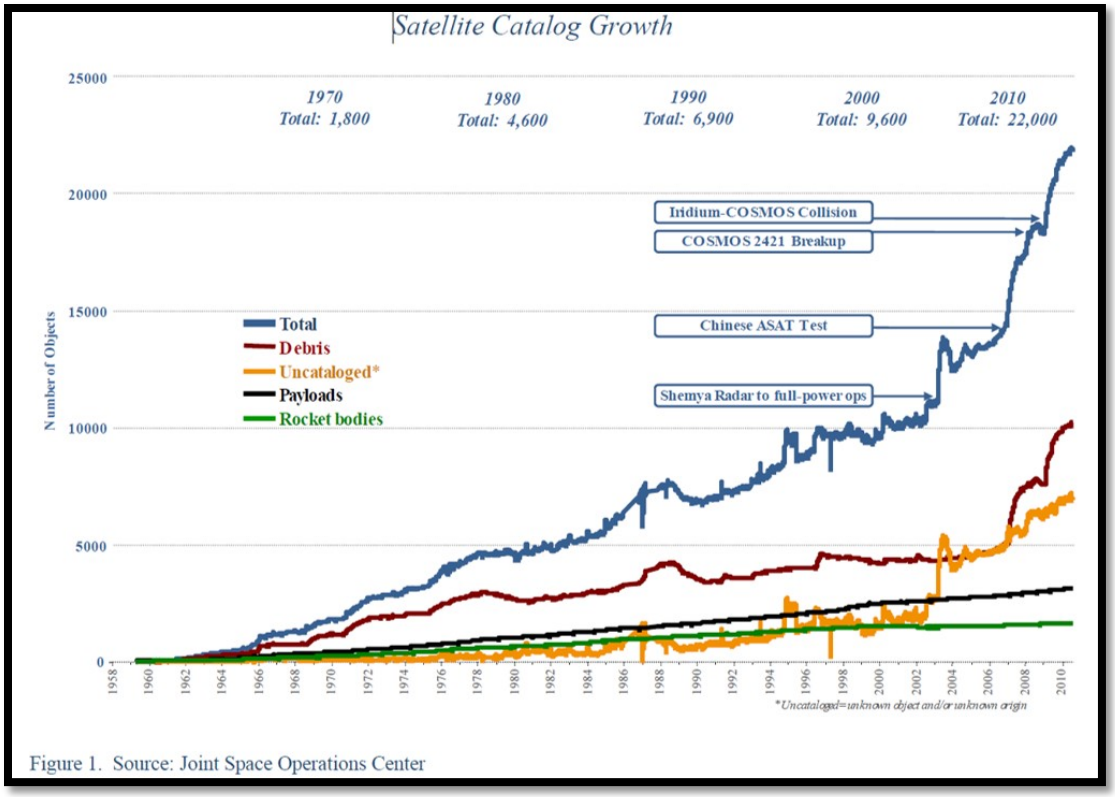

Figure 4: Satellite Growth Chart [1]

Modern approaches to understanding and determining satellite constellation orbits generally use only estimates of the orbital mechanics that include the two-body problem. The two-body problem might contain harmonic terms like Earth's gravitation potential up to a certain degree, but this numerical integration can have high residual error over long periods of time. For example the GPS ground receivers broadcast real-time ephemeris data that has a typical accuracy of less than one meter [8]. The data are only valid up to four hours before it needs to be updated as the ephemeris error will increase to almost six meters after just 24 hours. The National Geodetic Survey (NGS) has an accuracy of less than six cm [8]. However, NGS accuracy is obtained by calculating days of data from hundreds of reference stations. When

compared to current methods, increasing the accuracy of satellite constellation orbit determination over longer periods of time is the main motivation for this research [8].

1.6 Approach

To set the stage a short scenario of this research is explained in the following section. The goal is to place a constellation of satellites on a desired KAM torus so the satellites are drifting and following the same perturbations throughout the orbit over time. Placing all of the satellites on the same KAM torus will make orbital predictions more accurate, possibly out to years for an entire constellation. The satellite constellation is initially placed on a desired plane from the launch vehicle at specified increments. After all of the satellites have been placed two small delta-v maneuvers are implemented to insert each satellite onto a desired KAM torus that is nearby the initial launch plane. The desired KAM torus is known beforehand and gives mission planners the ability to predict accurate positions of the constellation so orbital maintenance will be minimal or possibly completely avoided and collision avoidance will be known possibly months in advance to allow for required orbital maneuvers that do not disrupt mission effectiveness.

This research uses a truth model from STK to create a desired orbit that demonstrates a typical trajectory that a small cluster or constellation of satellites would generally experience. STK extracts the COE from the orbit of just one satellite and uses the COE to determine the position and dynamics of the satellite over a week long orbit. Then, using the concept that the Earth's geopotential causes a constellation of satellites to rotate at three frequencies, anomalistic, precession, and apsidal, linear least squares approaches was used to determine those frequencies based on the ephemeris data from STK. Next, using the KAM torus theory

that those frequencies lie on a six dimensional torus, a satellite is placed on a new KAM torus using only two delta-v maneuvers from Wiesel's Two Impulse Maneuver Program [13]. The last position of the satellite is calculated after the maneuver and the satellite is propagated forward again. The COEs are extracted from STK by means of an ephemeris file and used to determine the three frequencies, using the linear least squares method a second time. Finally, the new frequency is compared to the desired torus frequency to see if the satellites new trajectory lies on the desired torus. The differences between these trajectories determine if the satellite is on the same KAM torus and will remain after a certain amount of time. This method could then be used to place multiple satellites on the same torus to increase the accuracy of satellite constellation orbit determination and predict accurate positions over longer periods of time using the KAM torus.

1.7 Problem Statement

Use a truth model in STK and osculating elements to insert a satellite onto a correct KAM torus at a specified position using the COEs. Ultimately, this method could be a practical approach to the wider astronautics community to calculate a more accurate satellite position and time over longer periods when compared to current orbital mechanics methods.

1.8 Investigative Questions

- Can accurate KAM Torus frequencies be modeled in STK using HPOP and derived from the linear least squares method?
- Can a satellite be placed on a desired KAM Torus with two delta-v maneuvers using the COEs?

1.9 Results

This research shows that inserting a satellite on a desired KAM torus using two delta-v maneuvers while modeling the scenario in STK does not create a precise representation of the desired trajectory. Extracting COEs from an STK model and calculating a KAM torus frequency from a linear least squares approximation creates a rough set of frequencies. The uncertainties presented in the KAM torus frequencies extracted from STK were excessive and did not create an accurate KAM torus to use for this analysis. The STK model frequencies were within 0.01 radians of the calculated secular drift rates. However, as the analysis shows, after a week propagation time the satellite would start to drift farther off the desired frequency, increasing the error.

II. Background

2.1 Chapter Overview

This chapter will begin with a short section on reference frames and Newton's three laws of motion; which will aid in understanding viewpoints of this research. Major perturbations experienced by satellites that orbit around Earth along with Earth's geopotential explanation will help the reader orient to the current issue. An explanation of the COE and how they are used to formulate the dynamics are reviewed. A section on orbital maneuvers and the rocket equation will clarify how they are being used in this research. Next, a summary of the current methods of satellite orbit determination, starting with the two-body problem, and Hamiltonian dynamics and ending with action-angle variables. A short history and description of KAM Theory will be explored. Finally, previous research from Wiesel and other students on KAM theory will be reviewed.

2.2 Reference Frames

Reference frames, the most fundamental idea in kinematics, form the basic building blocks of orbital dynamics, describing the orientation of a rigid body. The rigid-body model is a good approximation for studying spacecraft orientation despite the fact that a spacecraft is not in actuality a rigid-body [14]. In order to identify an object in space a coordinate system or reference frame needs to be defined. A reference frame normally has an origin that is the central location for all directions, and a set of basis vectors that define the path of that vector. The most common reference frame used is an inertial reference frame; non-rotating reference frame with the origin placed at the center and moving with a constant velocity (magnitude and direction) [15]. Any type of dynamics problem requires an inertial reference frame in order to

solve due to Newton's 2nd Law (explained in Section 2.3). The second type of reference frame is a rotating frame that rotates with respect to inertial space. A rotating reference frame

Table 1: Reference Frames [3]

Reference Frame	Type	Axis	Figure [3]
Earth-Centered Inertial (ECI)	Inertial (non-rotating)	I-axis – vernal equinox (fixed with respect to stars) K-axis – Earth's rotation axis (perpendicular to equatorial plane) J-axis – completes orthogonal right-handed frame	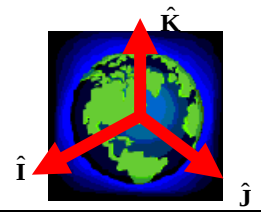
Earth-centered Earth Fixed (ECEF)	Non-inertial (rotating)	x-axis – Greenwich Meridian z-axis – Earth's rotation axis (perpendicular to equatorial plane) y-axis – completes orthogonal right-handed frame	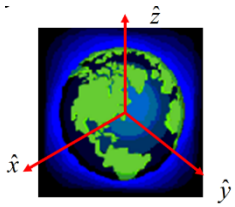
Perifocal	Inertial (non-rotating) dependent on certain orbit	P-axis – perigee direction W-axis – normal to orbital plane and out of the plane Q-axis – completes orthogonal, right-handed set of basis vectors	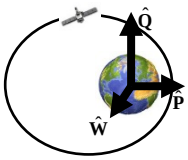
Body-fixed frame	Non-inertial (rotating) Attached to the satellite	Note: origin is generally at center of mass and axes are aligned with principal axes $(\widehat{b}_{,1}\ \hat{b}_2,\ \hat{b}_3)$	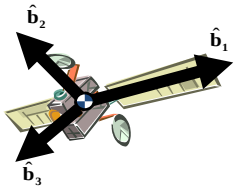
Orbital Frame	Non-inertial (rotating) centered on body and rotates as body moves along orbital path	O_3-axis – nadir direction (towards Earth center) O_2-axis – negative orbit normal direction O_1-axis – completes orthogonal, right-handed set (for circular orbits direction of the velocity orbit)	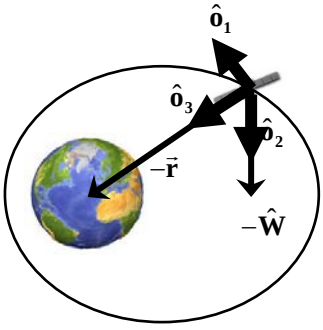

sometimes makes it easier to calculate distances and vectors between points but it is harder to visualize. Table 1 clarifies the different reference frames used in this research and the figures illustrate the frames further.

2.3 Newton's Three Laws of Motion

Newton's three laws of motion are the central concept behind orbit determination and give the basic foundation for the following concepts.

Newton's three laws of motion are as follows [16]:

1) If there is no applied force, an object will remain in whatever motion state it started in.
2) The sum of the applied forces on an object is equal to the time rate of change of momentum of that object.

$$\sum \vec{F} = m\vec{a} \qquad (1)$$

   Note: The mass is constant and acceleration $\vec{a}$ is inertial and taken with respect to an inertial reference frame.

3) For every applied force, there is an equal and opposite reaction force.

The first law is really a result of the second law in that if the sum of the applied forces is zero then there is no change in momentum. An object in motion will remain in motion at the same velocity as well. Equation (1) is really about position, velocity, acceleration and forces labeled as vectors; therefore in three-dimensional space the equation can be written as a sequence of three equations also known as the equations of motion [16].

2.4 Satellite Orbit Determination

Before his death in 1601, Tycho Brahe, an early Danish astronomer, challenged Johannes Kepler, a German mathematician, to estimate the orbit of Mars [17]. Kepler was inspired to examine one of the first orbit determination problems that led him to discover the following Laws: [17]

1) The orbits of the planets are ellipses with the Sun at one focus.
2) The line joining a planet to the Sun sweeps out equal areas in equal times.
3) The square of the orbital period- the time it takes to complete one orbit – is directly proportional to the cube of the mean or average distance between the Sun and the planet.

Kepler's three laws allowed scientists to predict not only orbits of planets but of moons and satellites that would later be proven by Isaac Newton. In 1665, Isaac Newton invented calculus, which enabled scientists to mathematically describe orbital motion, and he developed his famous law of gravitation, which would lead scientists to the ideal scenario of the restricted two-body problem [17]. The restricted two-body problem involves "two point masses orbiting under their mutual gravitation attraction" and is the only orbital motion problem with a closed form solution that allows scientists to analyze the motion of an orbiting object [18].

2.5 Two-Body Problem

To solve the two-body problem the positions of the two point masses are specified by R_1 and R_2 (seen in Figure 5). The masses are in an inertial reference frame, a frame that is not accelerating with inertial accelerations as $\ddot{R}_1$ and $\ddot{R}_2$.

Newton's second law is then applied to the two masses:

$$F_{12} = m_1 \ddot{R}_1 \quad (2)$$

$$F_{21} = m_2 \ddot{R}_2 \quad (3)$$

where F_{12} is the force on m_1 due to m_2 and F_{21} is the force on m_2 due to m_1.

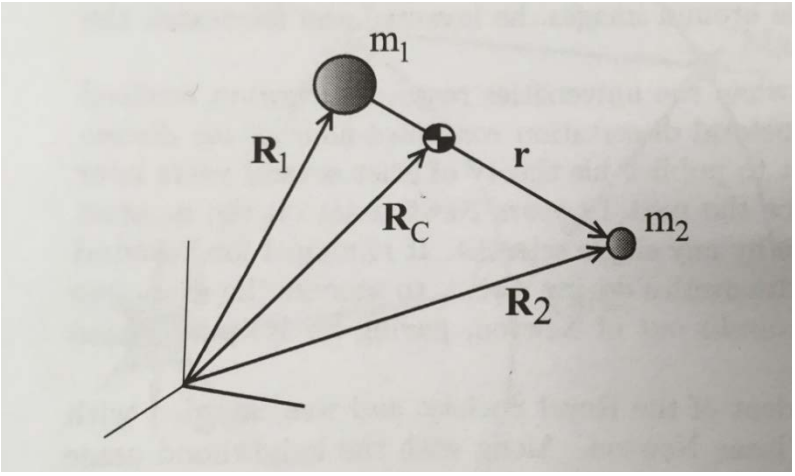

Figure 5: Two point masses in inertial reference frame [18]

Then setting these force equations equal to the gravitational force of the object yields:

$$m_1 \overrightarrow{\ddot{R}_1} = -\frac{G m_1 m_2}{\left|\vec{R}_1 - \vec{R}_2\right|^3}\left(\vec{R}_1 - \vec{R}_2\right) \quad (4)$$

$$m_2 \overrightarrow{\ddot{R}_2} = -\frac{G m_1 m_2}{\left|\vec{R}_1 - \vec{R}_2\right|^3}\left(\vec{R}_2 - \vec{R}_1\right) \quad (5)$$

When put into component form Equations (4) and (5) denote six second order, non-linear, coupled ordinary differential equations. Adding or subtracting these equations decouples them into two one-body problems, which can then be solved on their own.

Adding Equations (4) and (5) and introducing the center of mass vector $\vec{R}_c$ yields $\ddot{\vec{R}}$=0.

$$m_1 \ddot{R}_1 + m_2 \ddot{R}_2 = 0 \quad (6)$$

$$\vec{R}_c = \frac{m_1\vec{R}_1 + m_2\vec{R}_2}{m_1 + m_2} \quad (7)$$

From the $\ddot{\vec{R}}$ =0 Equation (6) can be integrated twice to show the velocity of the center of mass as a constant, and the momentum of $m_1\dot{R}_1 + m_2\dot{R}_2$ is also constant, therefore the position of the center of mass $\vec{R}_c$, can be determined at all times from the initial position.

$$R_c = \vec{R}_{c0} + \vec{V}_{c0}t \quad (8)$$

where $\vec{R}_{c0}$ is the initial position and $\vec{V}_{c0}$ is the velocity at time *t*. Equations (4) and (5) are half of the equations of motion needed to solve the two-body problem. The other half can be found by subtracting Equation (4) from Equation (5) and introducing the vector $\vec{r}$ between the two masses.

$$\vec{r} = \vec{R}_2 - \vec{R}_1 \quad (9)$$

To complete the equation multiply m_2 by Equations (4) and m_1 by Equations(5).

$$m_1 m_2 \ddot{r} = -\frac{Gm_1 m_2(m_1 + m_2)}{r^3}\vec{r} \quad (10)$$

Finally, if m_1 is Earth and m_2 is a satellite, the mass of the satellite would not be able to effect the drastically larger mass of Earth so only the product of Gm_1 is needed the following equation can be used as the other half of the two body problem:

$$\ddot{r} = -\frac{\mu\vec{r}}{r^3} \quad (11)$$

The gravitational parameter, μ, is used instead of *G* and m_1 because the parameter μ can be determined with higher precision than *G* or $m_1$by accurately tracking satellites. And finally, Equation (11) is the relative equation of motion for the two body problem.

2.6 Classic Orbital Elements

The two body problem is a dynamical system that has three degrees of freedom and the motion of two points (for example Earth and satellite) or the orbit of each can be completely described by the vectors *r*, *v* and an initial time t_0. The vectors *r* and *v* have three scalars each, making a total of six scalars that describe the motion of the orbit. This description is difficult to visualize so other forms of motion are used to describe an orbit that also need six scalar quantities; the COE is one primary example used [18].

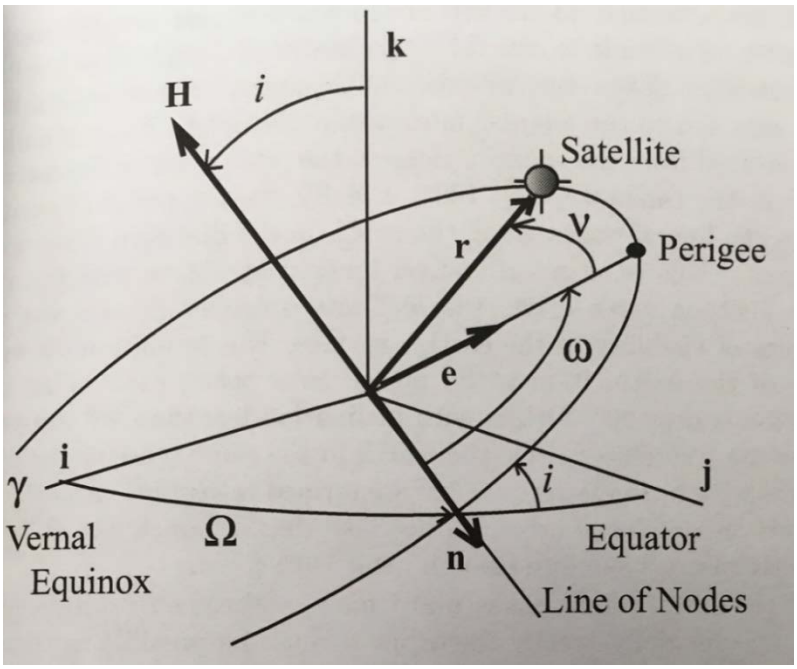

Figure 6: Classical Orbital Elements [18]

The first grouping of the COE describes the motion of the satellite within the orbital plane shown in Figure 6. The first element is denoted by *a*, the semi-major axis. It determines the size of the orbit and the orbital period. The second element in this section is the orbital eccentricity *e*, which determines the shape and type of conic section the orbit will be. The final element shown as T_0 is the time of perigee passage. The variable fixes the position of the satellite at one point in time and is used as a reference position of the satellite. The

corresponding angle to T_0 is the true anomaly, ν, which defines the position of the satellite moving along the orbit. It is the angle from the perigee position vector to the spacecraft position vector.

The next set of orbital elements defines the orientation of the orbit in space with respect to a reference frame. The inclination, *i*, describes the tilt of the orbital plane with respect to the equator. The angle is determined by using a vector, *k* perpendicular to the equator, and the vector *H*, which is perpendicular to the orbital plane. The next element is the right ascension of the ascending node (RAAN), Ω. The angle describes how the orbital plane is rotated in space or how it "swivels" in space. The RAAN uses the vernal equinox direction, denoted by *i*, as the starting point. Then the angle is measured eastward along the equator to the ascending node. The final element describes how the orbit is oriented within the orbital plane and is called the argument of perigee, ω. This angle is measured in the direction of the spacecraft's motion from the ascending node to perigee. Table 2 summarizes the COE in the ECI frame.

Table 2: Classical Orbital Elements [19]

Element	Description
a – semi-major axis	Defines the size and period of an orbit
e - eccentricity	Defines the shape of an orbit
v – true anomaly	Angle from the perigee position vector to the satellite's position vector (T_0) is the corresponding constant
i – inclination	Angle of the orbital plane with respect to the equatorial plane of the Earth
Ω - Right Ascension of the ascending node (RAAN)	Angle between the vernal equinox and the line of nodes
ω - Argument of perigee	Angle between the line of nodes and the perigee position

The COE gives the solution of the orbit at that specific time (which is only half of the solution). In order to determine the position and velocity of a spacecraft at any other time Kepler's Equation must be used. Five of the six COEs describe the shape and orientation of the orbit, but only one describes the satellite's location as a function of time. An elliptical orbit is not uniform so the true anomaly changes with time because it does not change consistently. Using Kepler's theory of planetary motion reveals the motion of a circle can be related to the motion on an ellipse using the variable *n* (labeled as the planet's mean motion). Figure 7 shows the auxiliary circle which contains the orbit ellipse and is tangent at two points.

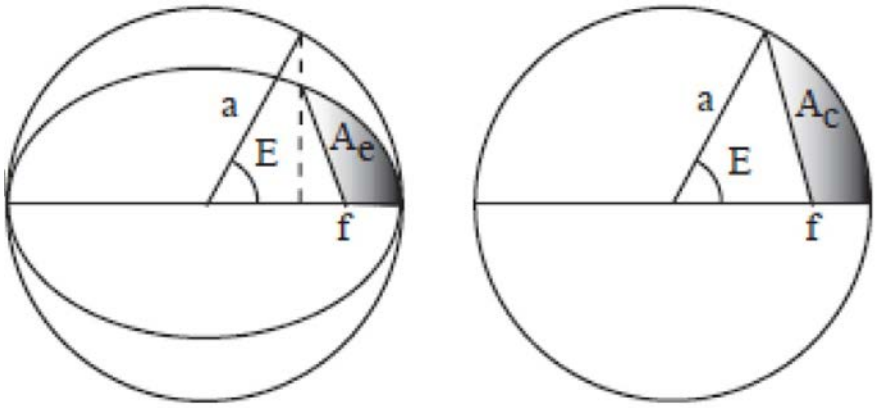

Figure 7: Kepler's Auxiliary Circles [18]

A new variable called the eccentric anomaly, *E*, helps compute the position of a point moving in a Keplerian orbit. Using Kepler's second law that the radius vector of an orbit sweeps out equal areas at equal times determines the area swept out by the radius vector denoted by A_e in Figure 7.

$$A_e = \frac{ab}{2}(E - e\sin E) \qquad (12)$$

where *b* is the semiminor axis calculated when you draw a triangle from each focus, *f* of the circle, to the end of the minor axis of the interior circle and solving for the third side. The eccentricity, *e*, as defined previously, and specifies the relative shape of the ellipse that can have a value on the interval of $0 \leq e \leq 1$. This is the area swept out by the satellite since perigee passage (T_0). The area the satellite sweeps out in one orbit is πab and the orbital period is

$$T = 2\pi\sqrt{\frac{a^3}{\mu}} \tag{13}$$

Now, using the concept that equal areas are swept out in equal times and setting the area of the ellipse over the time since perigee passage to the area swept out by the satellite over the period of the orbit gives the following ratio:

$$\frac{A_e}{t - T_0} = \frac{\pi ab}{T} \tag{14}$$

Replacing the area A_e and the period T will give the following equation:

$$\frac{\frac{ab}{2}(E - e\sin E)}{t - T_0} = \frac{\pi ab}{2\pi\sqrt{\frac{a^3}{\mu}}} \tag{15}$$

Canceling out a few variables and switching the radical leads to the following equation:

$$\sqrt{\frac{a^3}{\mu}}(t - T_0) = (E - e\sin E) \tag{16}$$

This leads to the final element, which can be defined as the mean anomaly. The mean anomaly, *M*, has no physical meaning and is difficult to show in a picture. However, it can be expressed mathematically by:

$$M = (E - e \sin E) \quad (17)$$

Kepler's Equation is a transcendental equation but when the equation is solved for E it does not give the angle which is required, the true anomaly, ν.

A relationship between E and ν can be seen by using the geometry of an ellipse inside the auxiliary circle again leading to the following equation:

$$\cos E = \frac{e + \cos \nu}{1 + \cos \nu} \quad (18)$$

Now using Equation (18) we can calculate ν if we have the time elapsed since periapsis passage. Periapsis is also referred to as perigee, as seen in Figure 6, is the point in the satellite's orbit at which the satellite reaches the closest distance to the center.

2.7 Major Perturbations on Earth-orbit satellites

The forces working against a spacecraft put into a specific orbit depend on the orbit where they are placed: Low Earth Orbit (LEO), Middle Earth Orbit (MEO), and Geostationary Equatorial Orbit (GEO). It is cheaper to send a satellite to a lower Earth orbit because it takes less propellant from a launch vehicle, but the mission does determine the orbit and what you need to do to keep that satellite within that orbit. All orbits experience a degree of these forces; some more than others.

LEO satellites (altitude between 160 – 2000 km) experience more atmospheric drag from the Earth's atmosphere because they are closer to the Earth. Therefore, they experience altitude decay where the satellite slowly loses altitude and moves closer to Earth after each orbit and slowly causes the orbit to become circular. These particular satellites need to perform more regular station-keeping maneuvers to keep them within the desired orbit. [18]

In GEO, (altitude greater than 35,786 km) there are forces that act to change the orbit over time. The Earth's orbit and the moon's orbit have an orbital plane and most GEO spacecraft are not aligned with that orbit so the sun and the moon will end up, over time, pulling on the satellite and possibly increase the satellite's orbital inclination. The Earth is also not shaped as a perfect circle. This causes the satellite to be drawn to a stable equilibrium point located along the equator, which will happen at about one degree of longitude per week. The North-South station keeping corrects the inclination deviations and East-West station keeping sustains the satellite at the original longitude within the GEO belt. [17]

A MEO region (altitude between 2000 – 35,785 km) is more commonly used for navigation, communication and science satellite missions. The higher altitude in MEO reduces the air drag from Earth's atmosphere to almost zero when compared to LEO satellites. However, MEO still experiences forces due to Earth oblateness which result in a rotation of the orbital plane and lines of nodes. Satellites in this region also experience increased speeds as it gets closer to the equator from the greater gravitation force and then a decrease in speed as the satellite moves away from the equatorial plane. Finally MEO also experiences smaller degrees of third body effects and solar radiation pressure when compared to GEO. [17]

2.8 Earth's Geopotential

The geopotential is described in orbital mechanics as the potential of the gravitational field of the Earth or the energy needed to keep an object gravitating around the Earth. The geopotential is normally defined by a series expansion into spherical harmonics taking into account the potential of the Earth's gravitational field and removing the centrifugal potential [20]. The Earth is not a perfect sphere and it actually resembles an ellipsoid with an equatorial

radius 20 km longer than its polar radius. Because of this shape the gravitation force is going to vary according to latitude, longitude and radial distance [18]. As explained in Section 2.4 the bulge creates a torque which results in the rotation of the orbital plane and the line of nodes. Finally, the satellite will experience increased speeds as it moves close to the equator and decreased speeds moving away as the gravity is pulling the satellite back towards the equator [17].

To derive the geopotential expansion around a solid body Poisson's equation for the gravitation potential V is used: [20]

$$\nabla^2 V = 4\pi G\rho \tag{19}$$

where G is Earth's gravitation constant, ρ is the density of the body, and ∇^2 is the Laplacian operator. Next, in spherical polar coordinates, with zero mass density, Poisson's equation becomes an infinite series expansion for the potential function outside of the gravitating sphere: (See Wiesel *Modern Astrodynamics* for a breakdown of the derivation.) [20]

$$V = -\frac{\mu}{r}\sum_{n=0}^{\infty}\sum_{m=0}^{n}\left(\frac{R_\oplus}{r}\right)^n P_n^m(\sin\delta)(C_{nm}\cos m\lambda + S_{nm}\sin m\lambda) \tag{20}$$

where μ is the gravitational parameter, r is the radius of the satellite from the Earth's center, $R_\oplus$ is the radius of the Earth, n and m are the degree and order of the expansion, P_n^m are the associated Legendre polynomials, C_{nm} and S_{nm} are the gravity field coefficients in terms of an Earth-gravity model, δ is the geocentric latitude and λ is the east longitude. The C_{22} term is the largest force that causes GEO satellites to drift in longitude. The C_{20} term is the Earth's oblateness and is related to J_2. [20]

2.9 Orbital Maneuvers

For the purposes of this research, a short summary of orbital maneuver is necessary to clarify the two-impulse maneuver strategy explained in Section 3.6. In spaceflight dynamics, orbital maneuvers are performed for two reasons; to maintain a specific orbit or transfer to a different orbit. A satellite is always under the influence of the gravitational field of a central body, like the Earth or the Sun, so spaceflight dynamics always needs to consider the laws of orbital motion when planning any orbital maneuver. In the case of this research, the two-body assumptions are used [18]. There are numerous ways to solve the orbital maneuver problem however, the problem normally centers on minimizing the propellant burned, or the Δv required for the maneuver. Additionally, when planning orbital maneuvers, there are two approaches: impulsive or continuous burns.

In order to maintain a specific orbit an impulsive burn is used. An impulsive burn is a simulation of a maneuver with an instantaneous change in the satellite's velocity, either magnitude and/or direction, but no change in the actual position. In reality, an instantaneous change is not realistic. This is a decent assumption considering the burn time of the rocket is much shorter than the actual orbit time, and the rockets used today have instant high thrust devices. A finite burn, sometimes called a non-impulsive burn, applies a low thrust over a longer period of time. This type of maneuver uses low thrust vehicles that can boost larger payloads into high-velocity payloads using a lot less fuel; however, the time to reach the desired position is much longer. [18]

The next type of orbital maneuver, the transfer orbit, moves a satellite from specified orbit trajectory to another orbit. The most notable transfer orbit is the Hohmann Transfer named after Walter Hohmann, a German scientist in 1925 [18]. This transfer orbit minimizes

the fuel burned and is the best two-burn instantaneous transfer between two coplanar circular orbits of different altitudes. Other orbit transfer maneuvers are the bi-elliptic transfer, which uses three delta-v engine burns to place the spacecraft from one orbit to another, and orbital inclination changes that require an increased amount of delta-v and is avoided by mission planners. The final orbital maneuver is a spacecraft rendezvous where two spacecraft arrive at the same point within an orbit in order to make contact. Rendezvous maneuvers require very precise timing and orbital velocity matches between the two spacecraft.

2.10 Rocket Equation

In order for a satellite to perform orbital maneuvers, it needs to fire some type of thruster to change its position. This is where the reaction force explained by the rocket equation comes in and why orbital mechanics needs to understand the implications of delta-v. Rocket propulsion is the preferred method of thrust used to launch a spacecraft into orbit and to maintain the orbit. The ideal rocket equation, or the Tsiolkovsky rocket equation, was derived and published by Russian scientist Konstantin Tsiolkovsky in 1903 [18]. It primarily follows the basic principle of conservation of momentum and the momentum exchange between the fuel that is expelled at high speed through a nozzle. The equation relates the delta-v, which literally means the change in velocity, with the effective exhaust velocity and the initial and final mass of the vehicle used [18]:

$$\Delta v = c \ln \frac{m_0}{m_1} \quad (21)$$

where c is the effective exhaust velocity, m_0 is the total initial mass (including the propellant), and m_1 is the total final mass. The specific impulse is also used as a measure how efficient the

rocket is and is defined by I_{sp} which basically means the "amount of momentum gained per unit weight of fuel consumed" [18]:

$$I_{sp} = \frac{c}{g_0} \quad (22)$$

where g_0 is the acceleration of gravity at sea level, is the effective exhaust velocity and the units of specific impulse are expressed in seconds.

When designing a satellite system, special care must be taken in the delta-v budget, which is a good indicator of how much propellant is required for the satellite's specific mission. Propellant usage is an exponential function of delta-v when reviewing the rocket equation (Equation (11)) and that is why specific orbital maneuvers like the Hohmann transfer (Section 2.9) are used to save on propellant consumption. The goal is ultimately, to save delta-v and attempt to do the maneuver with the least amount of propellant possible because the more propellant needed for a mission will also drive up the cost it takes to launch into space. The propellant needed for orbital station keeping can also not be replenished so designing a mission to meet the delta-v needs will aid in the mission lifetime of the satellite.

2.11 Hamiltonian Dynamics

There are a few methods to solving celestial mechanics problems that ultimately produce the same results with just different principles. The first one, as described above, using Newton's laws, specifically the second law, Equation (1), includes non-conservative forces that take into account constraint forces that can make it a little more complicated. Lagrangian mechanics, named after astronomer Joseph-Louis Lagrange in 1788, reformulates the classical mechanics approach by avoiding constraint forces, using a generalized coordinate system

instead and are better for conservative force systems [20]. Using modified Euler-Lagrange equations, the external forces can be separated into a sum of potential and kinetic forces with coordinates chosen to use symmetries in the system that make the motion of the system easier to solve. [21]

The Hamiltonian method, named after William Rowan Hamilton in 1833, uses Lagrangian mechanics and can be used to solve simple dynamic systems like harmonic oscillators but was created to solve more complex problems for celestial mechanics that can have multiple degrees of freedom and a convoluted time progression [18]. For example, the harmonic oscillator with a spring can be modeled as a Hamiltonian by taking into account the kinetic energy, *T*, and potential energy, *V*, of the spring in a rectangular coordinate frame in two dimensions. [20]

$$T = \frac{1}{2}m(\dot{x}^2 + \dot{y}^2) \tag{23}$$

$$V = \frac{1}{2}m(x^2 + y^2) \tag{24}$$

where *m* is the mass, *x* and *y* are the positions of the spring and $\dot{x}$ and $\dot{y}$ are the changes in distance over time. The Lagrangian function can be determined from $L = T - V$ and the momenta, $p_x = m\dot{x}$ and $p_y = m\dot{y}$, can be calculated by differentiating the Lagrangian, ∂L, with respect to the generalized velocities, $\dot{q}_i$. [20]

$$p_i(q_i, \dot{q}_i, t) = \frac{\partial L}{\partial \dot{q}_i} \tag{25}$$

The Hamiltonian can be calculated by using the designator *H* as the Legendre transformation of *L*.

$$H = \sum_i \dot{q}_i \frac{\partial L}{\partial \dot{q}_i} - L = \sum_i \dot{q}_i \, p_i - L \qquad (26)$$

The Hamiltonian Equation for a two dimensional harmonic oscillator can be formed by replacing the generalized velocities, $\dot{x}$ and $\dot{y}$ with the generalized momenta.

$$H = \frac{1}{2m}\left(p_x^2 + p_y^2\right) + \frac{1}{2}k(x^2 + y^2) \qquad (27)$$

In addition, Hamiltonian dynamics gives the ability to choose a coordinate frame that best meets the systems' needs, the Hamiltonian can also be formed using polar coordinates.

$$H = \frac{1}{2m}\left(p_r^2 + \frac{1}{r^2}p_\theta^2\right) + \frac{1}{2}kr^2 \qquad (28)$$

Next, in the Hamiltonian transformation, the canonical coordinates can be used to designate a system at any given point in time. The coordinates q_i and momenta p_i give the Hamiltonian system the ability to determine the velocity and momentum of every point uniquely.

$$\dot{q}_i = \frac{\partial H}{\partial p_i}, \quad \dot{p}_i = -\frac{\partial H}{\partial q_i} \qquad (29)$$

Equations (29) are the canonical equations of the Hamiltonian in first order differential equation form.

2.12 Canonical Transformations and Generating Functions

Canonical coordinates are created to localize a system within phase space or describe a physical system at any given point in time and are used in the Hamiltonian system. Canonical transformations is a method that allows for the change in one set of canonical coordinates and

momenta *(q, p)* to a new set of canonical coordinates and momenta *(Q, P)* while still maintaining the structure of the original Hamiltonian equations [21]. This method is useful when discussing the Hamilton-Jacobi equations.

In order to transform the coordinates a new Hamiltonian function, denoted by *K(Q, P)*, is defined, and the new coordinates *(Q, P)* will be given as a function of the original Hamiltonian equations, Equation (29). The new Hamiltonian function is denoted in Equation (30). [20]

$$\dot{Q}_i = \frac{\partial K}{\partial P_i}, \quad \dot{P}_i = -\frac{\partial K}{\partial Q_i} \tag{30}$$

The new variables *(Q, P)* must describe the same dynamical system as the old variables *(q, p)* to ensure a valid transformation. To show this the action integral (the system has a real number as the result and takes different values for different paths with dimensions of momentum by length), δ, over the Lagrangian $L_{qp} = \sum_i \dot{q}_i \, p_i - H$ and for the new system $L_{QP} = \sum_i \dot{Q}_i \, P_i - K$ must be equal to zero or static within the system. [21]

$$\delta \int (\sum_{i=1}^{N} \dot{q}_i p_i - H) \, dt = 0 \tag{31}$$

$$\delta \int (\sum_{i=1}^{N} \dot{Q}_i P_i - K) \, dt = 0 \tag{32}$$

For the new and the old system, the integral equal zero but that does not mean that the integrand of the new system is exactly equal to the integrand of the old system. The transformation between the two functions will be valid with an indirect generating function that can be determined from the relationship between the old and new coordinates. This generating

function's partial derivatives create the differential equations that determine a system's dynamics. [21]

$$\delta \int \left(\sum \dot{q}_i p_i - H(p_{i,} q_i, t) - \sum \dot{Q}_i P_i + K(P_{i,} Q, t) - \frac{dF}{dt} \right) dt = 0 \qquad (33)$$

The variation cancels out at the end times and becomes the following:

$$\delta \int_{t_1}^{t_2} \frac{dF}{dt} dt = \delta \big(F(t_2) - F(t_1) \big) = 0 \qquad (34)$$

The generating function needs to be identified in order for the transformation to be valid.

The old and new coordinates are independent so the $p_i = \frac{\partial F_i}{\partial q_i}$ and $P_i = -\frac{\partial F_i}{\partial Q_i}$ are used and the new Hamiltonian system *K* is related to the old system *H* by the next equation.

$$K(Q, P, t) = H(q, p, t) + \frac{\partial F_i}{\partial t} \qquad (35)$$

The next table shows the four basic generating functions for *F*.

Table 3: Canonical Transformations [20]

Generating Function	Derivatives of original	Derivatives of new
$F_1(q, Q, t)$	$p_i = \frac{\partial F_1}{\partial q_i}$	$P_i = -\frac{\partial F_1}{\partial Q_i}$
$F_2(q, P, t) = F_1 + QP$	$p_i = \frac{\partial F_2}{\partial q_i}$	$Q_i = -\frac{\partial F_2}{\partial P_i}$
$F_3(p, Q, t) = F_1 - qp$	$q_i = \frac{\partial F_3}{\partial p_i}$	$P_i = -\frac{\partial F_3}{\partial p_i}$
$F_4(p, P, T) = F_1 - qp + QP$	$q_i = \frac{\partial F_4}{\partial p_i}$	$Q_i = -\frac{\partial F_4}{\partial P_i}$

2.13 Hamiltonian-Jacobi Theory

The Hamiltonian-Jacobi Theory, named after William Rowan Hamilton and Carl Gustav Jacob Jacobi, defines the equations of motion for the Hamiltonian system [18]. When an accurate selection of coordinates is decided, the solution to the dynamical system can become simpler to obtain [21]. The theory is simpler when the coordinates are missing from the original Hamiltonian and when any of the momenta are missing from the new Hamiltonian, then the conjugate coordinate is constant. Equation (36) is the Hamilton-Jacobi equation and shows that the new coordinates and momenta are constant. [20]

$$H(q_i, p_i, t) + \frac{\partial F}{\partial t} = 0 \qquad (36)$$

And the equations of motion for the Hamiltonian are as follows:

$$\dot{Q}_i = \frac{\partial K}{\partial P_i} = 0 \qquad (37)$$

$$\dot{P}_i = \frac{\partial K}{\partial Q_i} = 0 \qquad (38)$$

Once again, a generating function is used to show the relationship between the old coordinates q_i and the new momenta, P_i. Reviewing Table 3 shows that the generating function, F_2, will yield the Hamilton-Jacobi Equation, Equation (36), and demonstrate the new Hamiltonian converts to Equation (39).

$$H\left(q_i, \frac{\partial F_2}{\partial q_i}\right) + \frac{\partial F_2}{\partial t} = 0 \qquad (39)$$

Equation (39) is usually referred to as Hamilton's Principal Function and it is a first-order, non-linear partial differential equation where the solution of the equation is commonly

denoted as $F_2 = S$. The integration of Equation (39) does not show how the new momenta are contained in *S* but only the dependence on previous coordinates and time [22].

A solution to Equation (39) can be shown in the following formula [22]:

$$S = S(q_1, \dots q_n; \alpha_q, \dots \alpha_n; t) \quad (40)$$

where q_n, are the variables for the partial differential equation in *n+1* variables and α_i are the n number of independent constants of the integration and *t* is time. Equation (40) is considered a complete solution where none of the *n* independent constants are solely additive, *S* is calculated in the form of the F_2 generating function, and, the new constant momenta are the constants of integration,

$$P_i = \alpha_i \quad (41)$$

Using the transformation equation from Table 3 for the F_2 generating function, the *N* transformation equations can be shown as [22]:

$$p_i = \frac{\partial S(q_i, \alpha_i, t)}{\partial q_i} \quad (42)$$

The second part of the transformation can also be obtained by using the F_2 generating function and shows the new constant coordinates as:

$$Q_i = \beta_i = \frac{\partial S(q_i, \alpha_i, t)}{\partial \alpha_i} \quad (43)$$

The constants α_i and β_i can be calculated by using the partial derivatives with the initial conditions at $t = t_0$ and the connected values of q_i. Finally, the Hamiltonian-Jacobi equation can be solved in terms of α, β, and *t* [22]:

$$q = q(\alpha, \beta, t) \quad (44)$$

Essentially the Hamilton's Principal Function changes the old system with variables to a new system with new coordinates and momenta that simplifies the equations of motion and enables the solution of the equations of motion [20]. The dynamical system is solved by using the Hamilton-Jacobi equation and the system shows that the coordinates and momenta are constant even in a new phase space [20].

2.14 Action-Angle Variables

In order to better visualize an invariant torus used in the KAM torus theory (explained in Section 2.15), a description of action-angle coordinates is necessary. The Hamilton-Jacobi theory described in Section 2.13 can be used to calculate frequencies of various motions without solving the equations of motion as long; as the system is separable and periodic. The action variables of the system are the integration constants, α_i, from Equation (40) referenced in Section 2.13 which are a set of independent functions.

Figure 8 describes the two types of periodic motion. The libration motion is also termed a harmonic oscillator and the system repeats the path for every point as q and p return to their original values after one period. The rotation motion as shown in Figure 8 shows q, the position coordinate, is an unbounded angle of rotation, which increases by the period q_0 where p is bounded for oscillation [22].

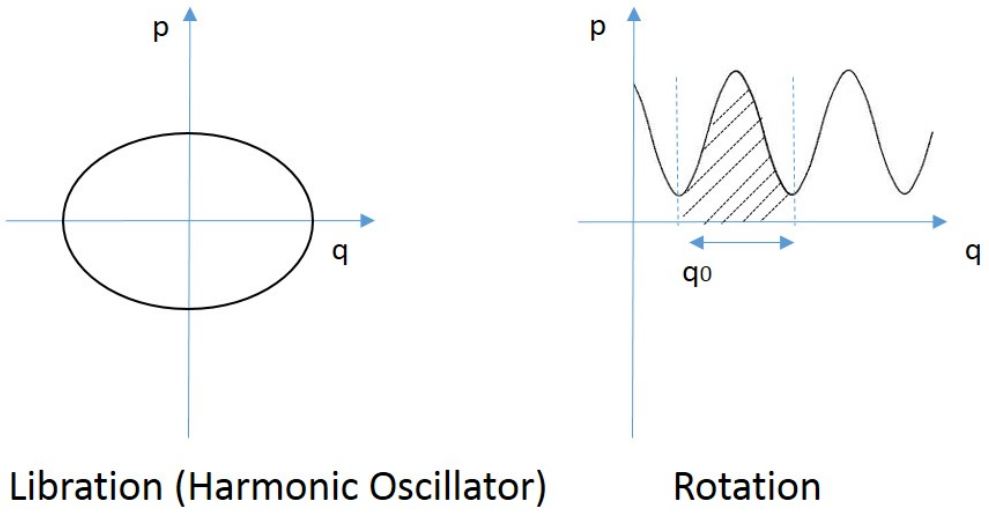

Figure 8: Periodic Motion

Action variable constants are usually defined by J_i, for either type of periodic motion and are the area in phase space taken over on period as illustrated by the shaded area in Figure 8 and shown in Equation (45) [22].

$$J_i = \oint p_i dq_i \tag{45}$$

Next, the action variables are changed using canonical transformation and the action angle variables w_i are the conjugate coordinates to the J_i.

$$p_i = \frac{\partial W}{\partial q_i} \tag{46}$$

$$w_i = \frac{\partial W}{\partial J_i} \tag{47}$$

where the solution is shown in Equation (37) is J_i as independent functions of α_i and W is the name of the characteristic function.

$$J_i = \oint \frac{\partial W(q_i, \alpha_i)}{\partial q_i} dq_i \quad (48)$$

Finally, action-angle variables can be used as the integration constants α_i from *S* in Equation (40) resulting in the characteristic function W.

$$W = W(q_1, \dots q_n; J_1, \dots J_n) \quad (49)$$

The variable w_i is repeated so the Hamilton-Jacobi equation is a function of only J_i which is equal to the constant α_i.

$$H = H(J_1, \dots J_n) \quad (50)$$

The Hamilton-Jacobi equations for the new set of variables w_i and J_i are [22]:

$$\dot{J}_i = \frac{\partial H}{\partial w_i} = 0 \quad (51)$$

$$\dot{w}_i = \frac{\partial H}{\partial J_i} = v_i \quad (52)$$

The variable v_i is the frequency of the periodic motion and the action-angle variables transformation calculates the frequencies. The v_i are constants of the motion of J_i so the angle variable are all linear functions of time yielding

$$w_i = v_i t + \beta_i \quad (53)$$

Equation (53) shows the angle variables increase linearly with time.

If the motion of the system is periodic, then in one period the entire system is

$$\Delta w_i = v_i \tau_i = 1 \quad (54)$$

where τ_i is the individual period of motion then

$$v_i = \frac{1}{\tau_i} \quad (55)$$

Equation (55) shows that $v_i$is indeed a frequency of the motion.

2.15 KAM Theory

The KAM theory stands for Kolmogorov, Arnold and Moser's contributions in Hamiltonian dynamical systems of quasi-periodic motions under small perturbations. The original problem was addressed by Andrey Kolmogorov in 1954, Jurgen Moser added to it with twist maps and finally the theory was proved for Hamiltonian Systems by Vladimir Arnold in 1963. [23]

Kolmogorov suggested two ideas [24]:

1. Linearize the problem about an approximate solution and solve the linearized problem
2. Improve the approximate solution by using the linearized problem solution as the basis of a Newton-Raphson method argument.

The KAM theory is really a set of methods developed into a large body of results that are related to quasiperiodic motions. In other words, for an integrable system in which the momenta and forces are invariant, or Hamiltonian, (subject to small smooth perturbations from conservative forces) many of the solutions for the unperturbed system are also solutions, with small changes, to the perturbed system [25]. The KAM theory ultimately describes the result of a perturbed integrable Hamiltonian system. The Hamiltonian can be written as [20]:

$$\mathcal{H}(J,w) = h(J) + \epsilon f(J,w) \qquad (56)$$

where *J* and *w* are the action-angle variables, *h* is the unperturbed Hamiltonian; f is the perturbing function, and finally ϵ is the small perturbing parameter. For example, if $\epsilon = 0$ the Hamiltonian equation reduces to the initial, integral system. Solutions to this Hamiltonian system are called torus because they have the characteristic of returning to their initial position

if one angular coordinate is increased by an integer multiple of some characteristic angular period and the other coordinates are held constant.

Integrable Hamiltonian plus small real perturbations lie on tori in phase space and remain upon the KAM tori for all time unless acted upon by a non-conservative force [26]. The KAM theory shows that when *n* constants of motion are known, the Hamiltonian system is integrable and has a phase space motion which lies on an n-dimensional torus in 2n-dimensional phase space. In this case n is the number of independent coordinates and action angles that can be used to describe the quasi-periodic motion, which describe integrable motion on the invariant torus [24]. If an object is on any of the trajectories within the invariant torus in phase space, it will stay on that torus [24].

A torus is defined as a surface of revolution and can simply be thought of as visually the product of N circles, when N is the dimension of the torus. A one-dimensional torus is a circle, and a two-dimensional torus is the shape of a ring or the product of two circles when the surface is formed by revolving one circle around the perimeter of another circle. The radius of the circle is denoted by *J* and the angle *w* is the angle between the vector from the center to a desired location on the outer line of the circle to some reference line as seen in Figure 9. The constant *J* and *w* are also termed the actions. Figure 10 shows pictures of the different dimensional tori and their actions.

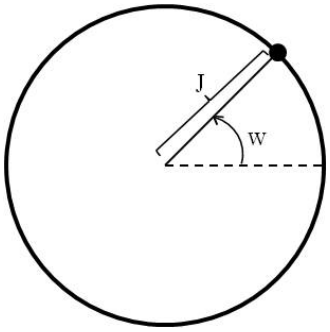

Figure 9: 1-Dimensional Torus [27]

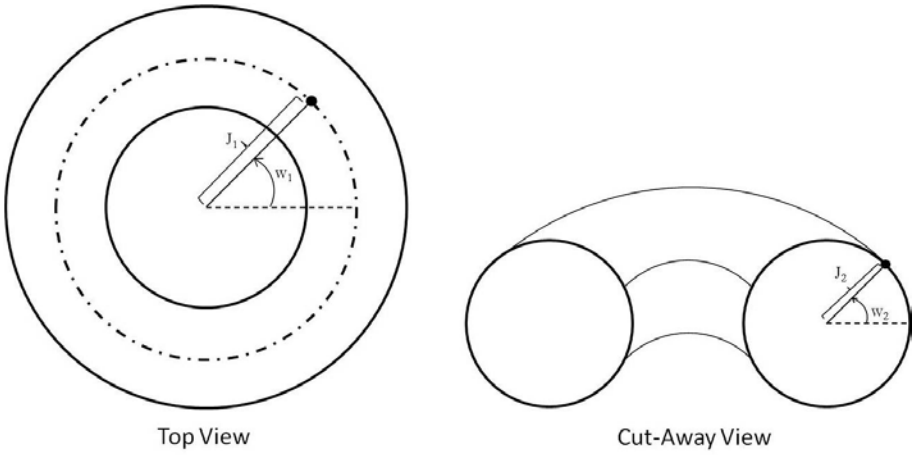

Figure 10: Multi-dimensional Torus [27]

Tori with higher dimensions are harder to visualize because they cannot be plainly drawn in three dimensional space. However, a satellite's orbit can be thought of as a three-dimensional torus (three-dimensions: a, e, and i) with a precessing argument of perigee, ω and a regressing node Ω as explained by Capt Frey in his thesis [27]. If the mean anomaly, *M*, is advanced by $n2\pi$, where n is an integer, and ω and Ω are held constant then the satellite will return to the exact position from which it started. This is also the same if any two of the three coordinates are held fixed while the third is incremented by 2π, the satellite's position will remain unchanged. Visually the satellite is following a 3-dimensional torus in 6-dimensional

phase space, with the dimensions being the angular coordinates and the three conjugate action momenta found from the Hamiltonian equations. [27]

A graph of a satellite orbiting a torus of a two month period can be seen in Figure 11 from 1st Lt Abay's thesis with the axis is kilometers in 3-D space [28].

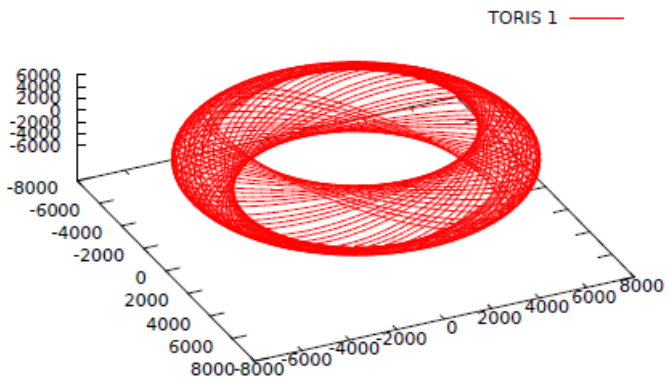

Figure 11: Satellite Orbiting a Torus [28]

2.16 Previous Research of KAM Torus

KAM Theory has definitely evolved over its 60 year history and shown a significant increase in the "understanding of the behavior of non-integrable Hamiltonian systems" [24]. However, KAM theory has never been applied to Earth orbiting satellites until Wiesel postulated in 2008 that three distinct fundamental frequencies observed in satellite motion, due to the Earth's known geopotential, could be the basis frequencies of a torus [29]. During his research, Wiesel was able to verify that Earth satellites lie on a KAM torus by numerically integrating an orbital trajectory using National Aeronautics and Space Administration's (NASA) Earth Gravitation Model 1996 (EGM-96) gravity model and then using Laskar frequency algorithms to determine the fundamental frequencies of the KAM torus [29]. Wiesel

then fit these frequencies to a Fourier series and used them to compare to a least squares approximation of the integrated orbit. The results showed evidence that Earth satellites do lie on a KAM torus with the resolution showing tens of meters after 20 days. Due to his conclusions, perturbation theory can use the torus as the exact solution to predict perturbations experienced by orbiting satellites rather than the Earth's geopotential [25].

The frequencies or the secular terms, as discussed in Wiesel's book *Modern Astrodynamics*, are already fundamentally used for Earth's geopotential [20]. First, the apsidal regression rate (movement of the argument of perigee), denoted by, $\dot{\omega}$, is the rotation rate of the orbit about its normal vector as seen in Equation (57). [20]

$$\dot{\omega} = -\frac{3nJ_2R_{\oplus}^2}{2a^2(1-e^2)^2}\left(\frac{5}{2}\sin^2 i - 2\right) \quad (57)$$

Where n is the mean motion, J_2 is the Earth geopotential factor, $R_{\oplus}$, is the radius of the Earth, a is the semi-major axis, e is the eccentricity of the orbit and i is the inclination. Next, the precession rate, denoted by, $\dot{\Omega}$, is the nodal regression rate and the Earth's rotation rate added together. The Earth's rotation rate is added because the term was placed in the ECEF reference frame. The precession rate can be seen in Equation (58). [20]

$$\dot{\Omega} = -\frac{3nJ_2R_{\oplus}^2}{2a^2(1-e^2)^2}\cos i \quad (58)$$

Finally, the Keplerian frequency, also called the anomalistic frequency, $\dot{M}$, is the resulting mean motion after taking into account the secular effects from the Earth's geopotential. The frequency can be seen in Equation (59). [20]

$$\dot{M} = -\frac{3nJ_2R_{\oplus}^2}{2a^2(1-e^2)^{\frac{3}{2}}}\left(\frac{3}{2}\sin^2 i - 1\right) \quad (59)$$

The secular rates exhibit many relationships that help explain some of the movements exhibited by Earth satellite dynamics. First, the anomalistic frequency decreases as the semi-major axis increases because Equation (59) is dominated by the mean motion. Second, the precession frequency, Equation (58), will become the Earth's rotation rate as the inclination approaches the 90 degree point. The nodal regression rate from the geopotential is removed because of the cosine term. Next, as the apsidal regression rate, Equation (57), goes to zero when the orbit approaches the critical inclination of 63.4 degrees. Craft concluded this in his thesis, *Formation Flight of Earth Satellites on KAM Tori* in 2009, that " accurate KAM tori may be constructed to characterize orbits with greater accuracy as long as certain constraints are used and accurate trajectories knowledge is obtained through numerical integration" [26]. The ultimate limitation of KAM torus construction is the extensive real-world trajectory history needed to calculate accurate KAM tori. More specifically, the accuracy of the KAM torus will decrease as the apsidal frequency, $\dot{\omega}$, goes to zero [26]. This relationship can also be seen clearly in Figure 12.

Other notable research can be seen from Frey's thesis, *KAM Torus Frequency Generation From Two-Line Element Set* in 2011. He explained how to accurately extract KAM Torus basis theory from a Two-Line Element (TLE) set. Small changes to the Torus basis frequency equals small changes in velocity. Moderate inclination and eccentricity values need to apply and air drag needs to be at a minimum and/or nearly constant. Future work suggestions were to survey satellites in a variety of orbits and review their limits of eccentricity, inclination and orbital period. [27]

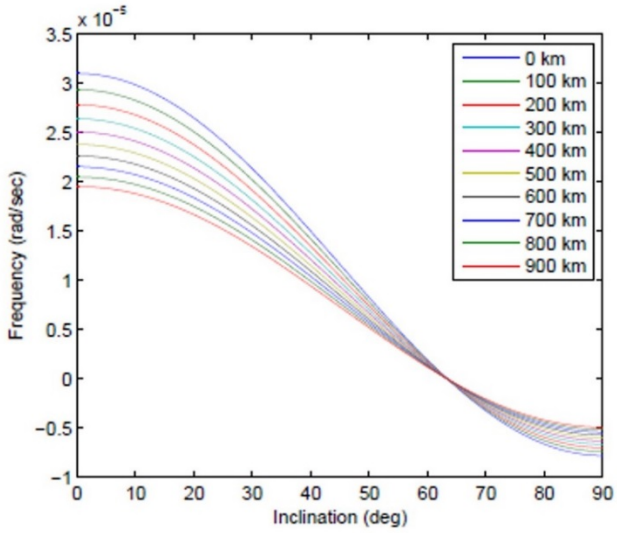

Figure 12: Apsidal Frequency vs Inclination in LEO [26] [30]

KAM theory can also be used to model dynamics for satellites in highly eccentric orbits with 0.5 meter accuracy, but with Earth's geopotential as the only perturbation used was proven by Dunk in *Applying KAM Theory to Highly Eccentric Orbits* in 2014. Dunk suggested comparing the position vectors of the same orbits with actual satellite data to ensure the accuracy of the KAM torus. [25]

Finally, Abay revealed in *KAM Torus Orbit Prediction From Two Line Element Set* in 2014, KAM torus orbit prediction is more accurate than Simplified General Perturbations 4 (SGP4) data. Using a periodic orbit with small perturbations, as low as 10^{-5}, and low eccentricities the KAM torus was fitted by least squares to the SGP4 and TLE data. The new method was more accurate compared to today's orbit prediction and numerical methods. [28]

III. Methodology

3.1 Chapter Overview

The chapter starts with a description of how orbital data were generated for this research analysis using STK as the orbit propagator using the Two Body Problem as a control model. Next, the methodology explains how a KAM torus frequency was calculated using the least squares method in MATLAB and how the state vector was defined at a specified position on a satellite orbit. Then, the KAM torus frequencies were used to generate an orbit transfer using Wiesel's two impulse maneuver strategy code [13]. From there a new position and velocity were used in the truth model, again in STK, to generate new ephemeris data to create new KAM torus frequencies using MATLAB.

3.2 Generating Orbital Data for Analysis

In order to test an orbital formation theory, orbital data must be acquired by either generating it from a program like Systems Tool Kit (STK) or using actual data from Two-Line-Element-Set (TLE). There are benefits and drawbacks for each type of method, but with today's model generators, a good integrator will allow the data to be matched with the KAM torus model generating only small errors. For this research a truth model was created in STK using the High Precision Orbit Propagator (HPOP). The HPOP uses numerical integration of the differential equations of motion to generate positions of a satellite at given times while taking into account different force modeling effects like a full gravitation field model (this research used WGS84 [World Geodetic System 1984] with nine terms), third-body gravity (this research used only the moon and the sun), atmospheric drag and solar radiation pressure [30]. The HPOP integration mode was used to give an orbit model as close to reality as possible. The

STK HPOP model provides more information during each integration step than just using the two-body problem propagator. The model was generated from the differential equations of motions that are integrated in HPOP, allowing for a precise orbit ephemeris generation [13].

The initial conditions for an orbit model were chosen based on several considerations:

1. Choose eccentric orbits greater than zero but less than 0.1 to create quantifiable frequencies
2. Start with an argument of perigee greater than 0 to create calculable frequencies
3. Choose an orbit above 550 km to avoid increased air drag but below 800 km for J2 effects
4. Choose an orbit in LEO to decrease third body effects and sun radiation perturbations
5. Inclination between the equator and 90 degree polar orbit was chosen

A MATLAB script was written to read in an excel file containing the raw ephemeris data from the STK model. All data were imported in degrees from 0 to 359. The values were converted to radians, and the 2π jumps were eliminated so the plots resulted in smooth lines of Mean Anomaly, RAAN, and argument of perigee as functions of time. Time for STK is imported as Coordinated Universal Time (UTC) and measured in mean solar days or 24 hour days rather than sidereal days, the time it takes the earth to rotate on its axis relative to the stars. The MATLAB script converted this raw time data to a continuous timescale, starting at zero, incremented in minutes and increasing throughout the entire orbit propagation.

3.3 Frequency Calculation

After the data was read-in and formatted with the MATLAB script, the characteristic frequencies for the orbit were determined:

$$\frac{\partial M}{\partial t}, \tag{60}$$

$$\frac{\partial \Omega}{\partial t}, \tag{61}$$

$$\frac{\partial \omega}{\partial t} \tag{62}$$

To calculate the frequencies a first order curve fit was accomplished using the least squares method. The following is an example of how the curve fit was implemented for each plot.

The data, or the smoothed angles calculated with the 2π jumps eliminated, are represented as a vector $\vec{y}$, while the time is denoted by the vector $\vec{t}$ and relates each data point. The variables a_i are the curve-fit coefficients. The curve will be in the form of:

$$\vec{y} = a_0 + a_1\vec{t} \tag{63}$$

Next, a matrix T is expressed as

$$T = \frac{\partial \vec{y}}{\partial a_i} = [1 \quad t] \tag{64}$$

where $\vec{1}$ is a column vector of the same length of $\vec{t}$ containing all ones. The curve-fit coefficients are solved by

$$\vec{a} = (T^T Q^{-1} T)^{-1} T^T Q^{-1} \vec{y} \tag{65}$$

where Q is the covariance matrix, but assumed to be an identity matrix because the individual data points are not known. The curve fit is given by

$$\vec{f} = T\vec{a} \tag{66}$$

And residuals, $\vec{r}$, can be calculated:

$$\vec{r} = \vec{y} - \vec{f} \tag{67}$$

To determine the accuracy of the curve-fit, the covariance matrix, $\vec{P}$ was determined

$$\vec{P} = (T^T Q^{-1} T)^{-1} \vec{r}_0 \tag{68}$$

where $\vec{r}_0$ is the average squared residual, that can be approximated by the standard deviation squared, σ^2 and N is the number of data points. [20]

$$\vec{r}_0 = {}^1/_N \sum_{i=1}^{N} \vec{r}_i^2 \sim \sigma^2 \tag{69}$$

A MATLAB script was created to implement this calculation and output the two variables a_0 and a_1. The slope value, a_0 was used as the value for each of the three frequencies.

3.4 State Vector Definition

Now that the frequencies have been determined as a function of the COE, a state vector can be defined with six scalars that describe the motion of the orbit as explained in the COE section. The state vector will consist of the three angles M, Ω, ω and their angular rates in place of the elements $a, e,$ and i.

$$\vec{X} = \begin{Bmatrix} \theta_1 = M \\ \theta_2 = \Omega \\ \theta_3 = \omega \\ \omega_1 = \dot{M} \\ \omega_2 = \dot{\Omega} \\ \omega_3 = \dot{\omega} \end{Bmatrix} \tag{70}$$

Next, using the new state vector, a matrix of the angles and angular rates can be defined.

$$\frac{\partial \vec{\omega}}{\partial(a,e,i)} \tag{71}$$

The inverse of this, calculated numerically, can be used to change the classical element partials matrix into the following form:

$$\frac{\partial(\vec{r},\vec{v})}{\partial(\vec{\theta},\vec{\omega})} = \frac{\partial(\vec{r},\vec{v})}{\partial(M,\Omega,\omega,a,e,i)} \frac{\partial(M,\Omega,\omega,a,e,i)}{\partial(\vec{\theta},\vec{\omega})} = \frac{\partial(\vec{r},\vec{v})}{\partial(M,\Omega,\omega,a,e,i)} \begin{Bmatrix} I & 0 \\ 0 & \frac{\partial(a,e,i)}{\partial \vec{\omega}} \end{Bmatrix} \tag{72}$$

3.5 New Torus Definition

The goal of this research is to place a constellation of satellites on a desired KAM torus so the satellites are drifting and following the same perturbations throughout the orbit over time. The STK truth model generated precise ephemeris data that was used to calculate the KAM torus frequency that the satellite was currently on. A new KAM torus frequency set was defined based on the truth model KAM torus. This is labeled as the desired KAM torus. The desired torus frequency set attempted to set a satellite on a specific KAM torus and this was logically defined by zeros after the seventh term in *M* and ω terms and in the eighth term in the Ω term for the first test. This KAM torus is not necessarily less accurate but it is the chosen insertion rate to test if the satellite is following frequency and phase of the rest of the satellites on that torus.

The difference between the desired KAM torus and the calculated truth model is as small as a half meter because the launch vehicle has already placed all of the satellites in the constellation on the desired plane and as close to the desired KAM torus as the accuracy of the launch vehicle will allow. After all of the satellites have been placed the two, very small, delta-v maneuvers should just nudge or insert each satellite onto the nearby desired KAM torus. The

maneuvers are kept small to use the least amount of propulsion on the satellites as explained by Sections 2.9 and 2.10.

3.6 Two Impulse Maneuver Strategy

In order to place a satellite on the suitable trajectory so it will lie on the desired torus the current satellite will need to perform a two-impulse delta-v maneuver from its current trajectory. The current trajectory is the truth model created in STK (explained in Section 3.2). The satellite will be placed on a new trajectory using the desired KAM torus state vector (explained in Section 4.2.2.). In order to determine the two impulse maneuver strategy, the KAM torus state of angles and frequencies, was input into a numerical integration routine developed by Wiesel [13], which calculates the best delta-v in order to decrease the maneuver cost to the lowest amount possible. The routine uses the two body model with J_2 corrections to the rates of mean anomaly, RAAN, and the argument of perigee. The program calculates a delta-v at each point and determines at which point will be the maneuver that will have the smallest delta-v. The program limited the time to half a day calculations.

The physical state of the satellite is represented by the following equation:

$$X^T = (\vec{r}, \vec{v}) \tag{73}$$

where $\vec{r}$ is the position and $\vec{v}$ is the velocity of the satellite in the ECEF frame. The KAM torus state is shown in Equation 74 where $\vec{\theta}$ are the three angles anomalistic, precession, and apsidal, while $\vec{\omega}$ are the changes of those angles over time.

$$Y^T = \left(\vec{\theta}, \vec{\omega}\right) \tag{74}$$

In addition, there is the relationship between the small changes in the physical and KAM states denoted by Equation 75

$$\delta X(t) = \frac{\partial X(t)}{\partial Y(t)} \delta Y(t) \quad (75)$$

where the $\delta X(t)$ term is the change in physical state of the satellite is equal to the partial derivatives of the physical state $\partial X(t)$, divided by the KAM torus states $\partial Y(t)$ multiplied by the differential of the KAM torus state $\delta Y(t)$.

The solution in the KAM variables is the linear drift and constant behavior equation:

$$Y(t_1) = Y(t_0) + \begin{pmatrix} \omega(t_1 - t_0) \\ 0 \end{pmatrix} \quad (76)$$

where $Y(t_1)$ is the position of the KAM torus at the first position and $Y(t_0)$ is the initial position. The change in position $\begin{pmatrix} \omega(t_1 - t_0) \\ 0 \end{pmatrix}$ is the frequency, ω, of the KAM torus state multiplied by the change in time, and 0 denotes there is no change in the frequency. This gives the KAM torus state transition matrix:

$$\Phi_Y(t_2, t_1) = \begin{Bmatrix} I & I(t_2 - t_1) \\ 0 & I \end{Bmatrix} \quad (77)$$

where Φ comes from linear dynamical systems and Φ propagates the actual states as a function of time not the differential of the state. I is the identity matrix with initial conditions $\phi(t_0, t_0) = I$.

Two maneuvers will be performed at t_1, and t_2,where: $t_0 < t_1 < t_2 < t_{max}$ and t_0, is the time at the initial position. Given changes in the KAM torus state are going to be evaluated at some upper limit time labeled t_{max}.

$$\Delta Y(t_{max}) = \begin{pmatrix} \Delta\theta \\ \Delta\omega \end{pmatrix} \quad (78)$$

where $\Delta\theta$ is the change in three angles and $\Delta\omega$ is the change in frequencies from the initial time to the upper limit time. This maneuver will be done in four phases.

Phase One: First, the satellite drifts from the start time $t_{0,}$ to the time of the first maneuver, $t_{1,}$. The torus state changes as:

$$Y(t_1^-) = Y(t_0) + \begin{pmatrix} \omega_0(t_1 - t_0) \\ 0 \end{pmatrix} \quad (79)$$

where t_1^- denotes the state of the KAM torus before the first maneuver, and ω_0 is the initial frequency of the KAM torus.

Phase Two: The first maneuver is performed with instantaneous change in position and an unknown maneuver vector Δv_1. This gives the relation between the physical and torus states as:

$$\Delta X(t_1) = \begin{pmatrix} \Delta r = 0 \\ \Delta v_1 \end{pmatrix} = \frac{\partial X(t_1)}{\partial Y(t_1)} \begin{pmatrix} \Delta\theta_1 \\ \Delta\omega_1 \end{pmatrix} \quad (80)$$

where $\Delta r = 0$ is the initial position. This gives the torus state changes as:

$$\begin{pmatrix} \Delta\theta_1 \\ \Delta\omega_1 \end{pmatrix} = \left\{ \frac{\partial X(t_1)}{\partial Y(t_1)} \right\}^{-1} \begin{pmatrix} 0 \\ \Delta v_1 \end{pmatrix} \quad (81)$$

Partition the inverse matrix to find the coefficients of the state changes in more detail:

$$\begin{pmatrix} \Delta\theta_1 \\ \Delta\omega_1 \end{pmatrix} = \begin{Bmatrix} A_1 & B_1 \\ C_1 & D_1 \end{Bmatrix} \begin{pmatrix} 0 \\ \Delta v_1 \end{pmatrix} = \begin{pmatrix} B_1 \Delta v_1 \\ D_1 \Delta v_1 \end{pmatrix} \quad (82)$$

Phase Three: The satellite will drift on the new torus for a specific time and then meet the time just before the second maneuver denoted as t_2^-. The following equation is the state just before the second maneuver:

$$\begin{aligned} Y(t_2^-) &= Y(t_1^+) + \begin{pmatrix} (\omega_0 + \Delta\omega_1)(t_2 - t_1) \\ 0 \end{pmatrix} + \begin{pmatrix} \Delta\theta_1 \\ \Delta\omega_1 \end{pmatrix} \\ &= Y(t_0) + \begin{pmatrix} \omega_0(t_2 - t_0) \\ 0 \end{pmatrix} + \begin{pmatrix} (B_1 + D_1(t_2 - t_1))\Delta v_1 \\ D_1 \Delta v_1 \end{pmatrix} \end{aligned} \quad (83)$$

Phase Four: The second maneuver then changes this to a new torus state:

$$\Delta Y_2 = \begin{pmatrix} \Delta\theta_2 \\ \Delta\omega_2 \end{pmatrix} = \begin{pmatrix} B_2\Delta v_2 \\ D_2\Delta v_2 \end{pmatrix} \tag{84}$$

A final drift to the end time could be added, but it is not necessary, because at this point the correct torus has been achieved. The final state after the second maneuver is:

$$\begin{aligned} Y(t_2^+) = Y(t_0) &+ \begin{pmatrix} \omega_0(t_2 - t_0) \\ 0 \end{pmatrix} \\ &+ \begin{pmatrix} (B_1 + D_1(t_2 - t_1))\Delta v_1 \\ D_1\Delta v_1 \end{pmatrix} \\ &+ \begin{pmatrix} B_2\Delta v_2 \\ D_2\Delta v_2 \end{pmatrix} \end{aligned} \tag{85}$$

The first two terms on the right of the equal sign are the natural drift that would have occurred without maneuvering. The last two terms give the changes the torus state needs:

$$\Delta Y(t_{max}) = \begin{pmatrix} \Delta\theta \\ \Delta\omega \end{pmatrix} = \begin{pmatrix} (B_1 + D_1(t_2 - t_1))\Delta v_1 \\ D_1\Delta v_1 \end{pmatrix} + \begin{pmatrix} B_2\Delta v_2 \\ D_2\Delta v_2 \end{pmatrix} \tag{86}$$

This rearranges to give a single sixth order matrix equation for both maneuvers:

$$\begin{Bmatrix} B_1 + D_1(t_2 - t_1) & B_2 \\ D_1 & D_2 \end{Bmatrix} \begin{pmatrix} \Delta v_1 \\ \Delta v_2 \end{pmatrix} = \begin{pmatrix} \Delta\theta \\ \Delta\omega \end{pmatrix} \tag{87}$$

3.7 Canonical Units

During the analysis of this research, canonical units were used to define objects within the reference orbit. Canonical units, which make the calculations easier to perform, are convenient in astrodynamics when the exact distances and masses of objects are not known. Table 4the quantities used in the canonical unit's calculations:

Table 4: Canonical Units

Type	**Value**	**Units**
Time Unit (TU)	13.44686457	Min/TU
Distance Unit (DU)	6378.135	Km/DU

3.8 New Position and Velocity determination

Wiesel's numerical integration routine outputs the best times to complete maneuvers one and two along with the delta-v required for each maneuver in canonical units. The values were then converted to minutes for the time and velocities with units of kilometers per second to be used in the STK program. All calculations were done in MATLAB with output display format set to long for 15 digits after the decimal point for greater accuracy.

After the velocities and times were determined the values were entered into STK. In the STK model a new satellite was created to start at the first maneuver time. The delta-v maneuver was assumed to be impulsive so the position was not changed at the first maneuver time, but the new velocity was entered into the ECI frame. STK only allows for up to seven significant digits entered into the program for any given vector value.

The second satellite was propagated forward to the second maneuver time and then a third satellite was created to start at the position of the second maneuver time. The second maneuver velocity was entered into the velocity components, and the position did not change as the maneuver is instantaneous. The satellite was then propagated forward for a certain time in order to generate ephemeris data for a new KAM torus frequency calculation.

3.9 New Frequency Calculation and Error Residuals

A new ephemeris file was created from the third satellite after a certain propagation time. The new ephemeris files were downloaded into MATLAB and the three KAM torus frequencies were then calculated again using the same least squares method as described in Section 3.3. The least squares method in MATLAB also produced the error residuals used in the analysis.

IV. Results

4.1 Chapter Overview

The following chapter will describe the truth model used for the test satellites and the issues that were discovered during the process. This chapter will also show the results from the process described in Chapter III for frequencies generated from the STK model and MATLAB calculations.

4.2 First Test Case (1 week initial propagation)

The first test case proposed was a one week satellite propagation time in STK to create an ephemeris file that generated the classical orbital elements (COE) of the satellite at every minute of the orbit. Table 5 shows the satellite properties used for Test Case 1.

Table 5: Case 1 Orbital Parameters Test Case 1

Parameter	Value
Propagation Time	8 days
Semi-major Axis	6928.14 km
Eccentricity	0.03
Inclination	50 deg
Argument of Perigee	30 deg
RAAN	0 deg
True Anomaly	360 deg

4.2.1. Initial Frequency Calculations

The data curve fit graphs for the three KAM torus frequencies, *M*, Ω, and ω can be seen in Figure 12 through Figure 17 along with the residuals. The residuals for the Mean Anomaly, *M*, and the Argument of Perigee, ω, were small and varied between +/- 0.02 radians. The residuals for RAAN can be seen closer in Figure 18 and were consistently +0.004 radians and decreasing to -.002 radians by the end of the propagation time.

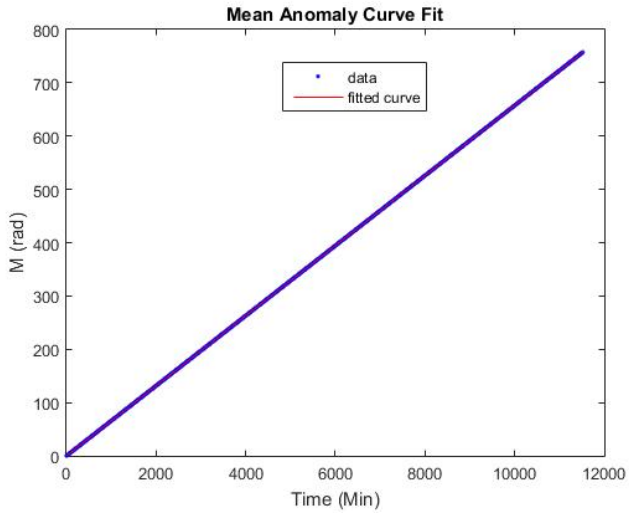

Figure 13: Mean Anomaly Curve Fit

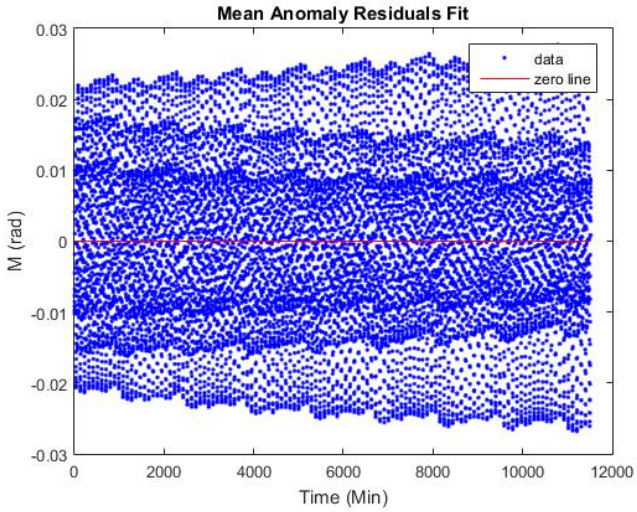

Figure 14: Mean Anomaly Residuals Fit

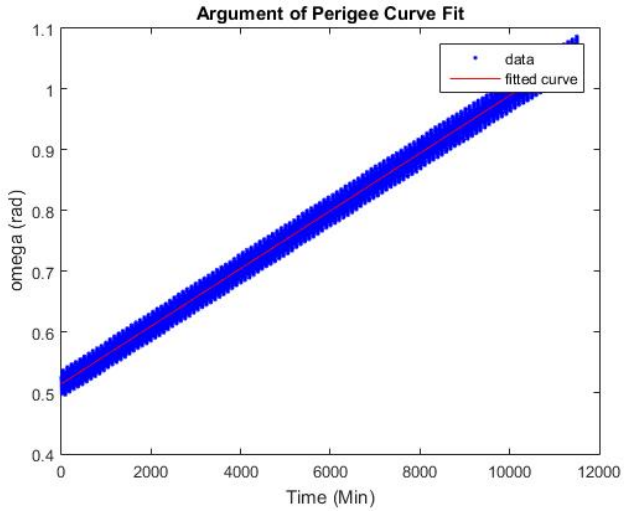

Figure 15: Argument of Perigee Curve Fit

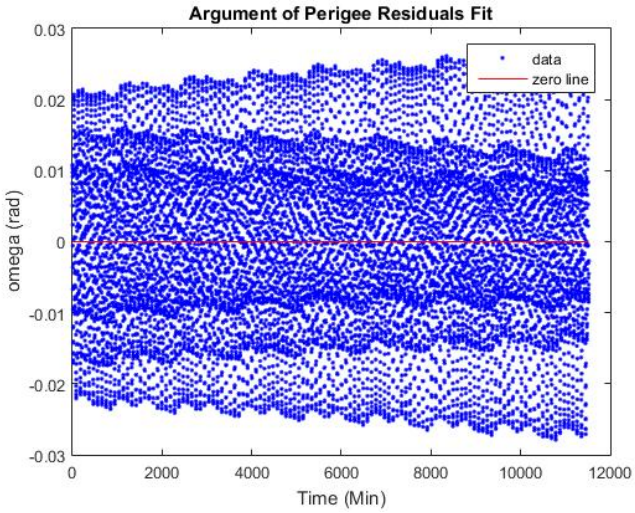

Figure 16: Argument of Perigee Residuals

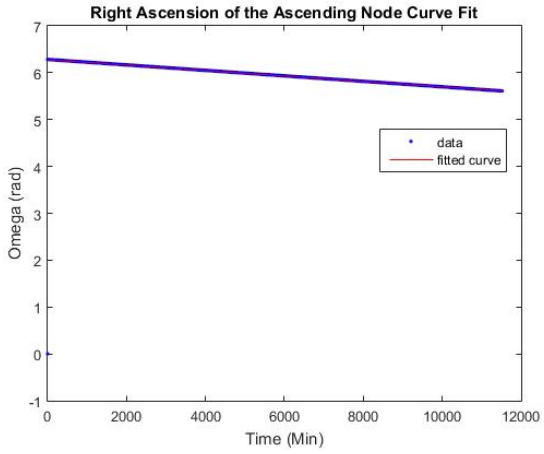

Figure 17: RAAN Curve Fit

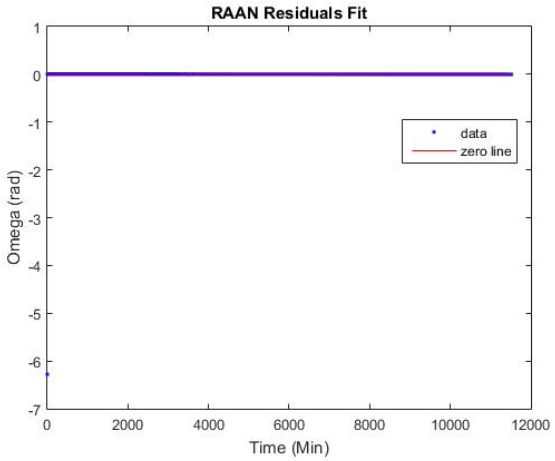

Figure 18: RAAN Residuals Fit

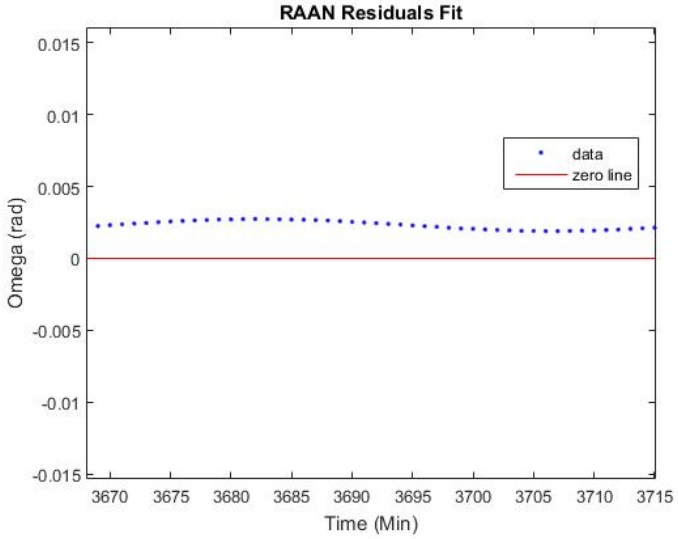

Figure 19: RAAN Residuals Fit Zoomed in

The curve fit data can be seen in numerical form in Table 6:

Table 6: Curve Fit Data

Angle	a_0 (rad/min)	a_1 (rad)
M	0.065745761368609	-0.058064167536148
Ω	-0.000057799119548	6.278530657747206
ω	0.000047435106094	0.515341711548231

4.2.2. New KAM torus frequency

The KAM torus frequencies were altered from the truth model to the new KAM torus frequencies as shown in Table 7. The new frequencies had a difference of 10^{-8} for the Mean Anomaly, 10^{-10} for the RAAN, and 10^{-9} for the argument of perigee.

Table 7: New KAM Torus Frequencies

Angle	Desired Frequency	Initial Frequency	Difference
M	0.06574570000000	0.06574576136860	-6.14E-08
Ω	-0.00005780000000	-0.00005779912000	-8.80E-10
ω	0.00004744000000	0.00004743510600	4.89E-09

4.2.3. The Two Impulse Maneuver Data

The two impulse maneuver program output the following data for the two maneuvers in Table 8:

Table 8: Impulse Maneuver Data

	1st Maneuver	**2nd Maneuver**
Time (TU)	1 hr 40 min 14.42 sec	4 hrs 6 min 56 sec
$V\hat{\imath}\left({}^{km}/_{s}\right)$	5.91095e-04	-5.28705e-04
$V\hat{\jmath}\left({}^{km}/_{s}\right)$	5.85915e-04	-1.29687e-03
$V\hat{k}\left({}^{km}/_{s}\right)$	2.65510e-04	-4.55767e-04

The maneuver cost graph shows the time before the first maneuver as t_1 along the horizontal (normally x) axis and time before the second maneuver and after the first as t_2 along the second horizontal axis (normally y-axis). The delta-v variable along the vertical axis (normally the z-axis) is in units of km/s. The maneuver cost graph is shown in Figure 19:

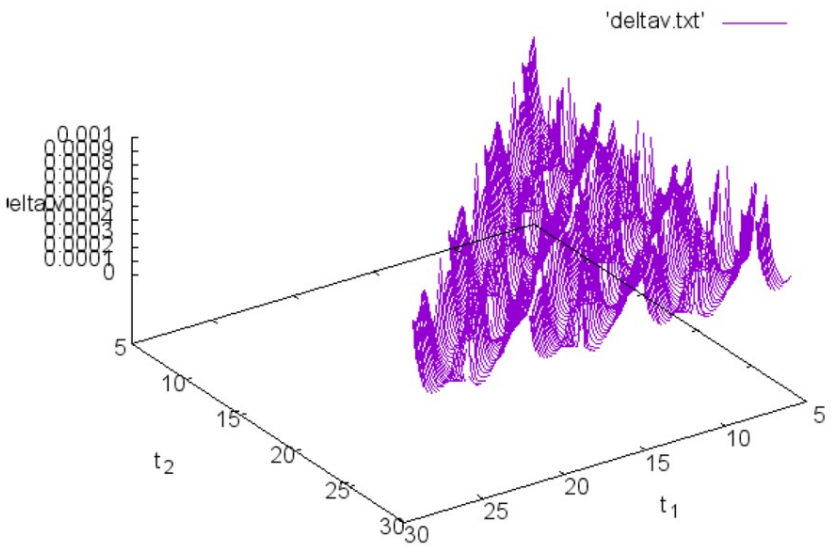

Figure 20: Maneuver Cost Graph Test Case 1 [13]

The program created by Wiesel (explained in Section 3.6) attempted to find the least delta-v at each point along the maneuver time. The trough and peaks within the graph show an orbit and the delta-v needed increases the more orbits pass. The program chose the delta-v that is in the valley to find the least amount of delta-v used. There is a 45 degree cut-off in the graph because t_1 needs to happen before t_2. Therefore, there is a skewed appearance to the graph.

4.2.4. New Frequency Calculations

The new KAM torus frequencies were calculated at three different propagation times (one, two and three weeks) to determine if the frequency would fall onto the desired KAM torus

Table 9: New Curve Fit Data

Angle	New	Difference from desired
M (desired)	0.06574570000000	0.00E+00
M (initial)	0.06574576136860	-6.14E-08
M (1 week)	0.06574266634540	-3.03E-06
M (2 weeks)	0.06574270786501	-2.99E-06
M (3 weeks)	0.06574264000881	-3.06E-06
M Secular Rate before maneuver	0.06636014962052	6.14E-04
M Secular Rate after maneuver	0.06636333728480	6.18E-04
Ω (desired)	-0.00005780000000	0.00E+00
Ω (initial)	-0.00005779912000	-8.80E-10
Ω (1 week)	-0.00005840561997	-6.06E-07
Ω (2 weeks)	-0.00005841383507	-6.14E-07
Ω (3 weeks)	-0.00005841510573	-6.15E-07
Ω Secular Rate before maneuver	-0.00005560411135	2.20E-06
Ω Secular Rate after maneuver	-0.00005565571270	2.14E-06
ω (desired)	0.00004744000000	0.00E+00
ω (initial)	0.00004743510600	4.89E-09
ω (1 week)	0.00004718192930	-2.58E-07
ω (2 weeks)	0.00004715731676	-2.83E-07
ω (3 weeks)	0.00004723059206	-2.09E-07
ω Secular Rate before maneuver	0.00004621412693	-1.23E-06
ω Secular Rate after maneuver	0.00004639437143	-1.05E-06

value as the satellite propagated along the torus. Table 9 lists the data. The desired frequency is listed first with the initial calculated frequencies from the least squares approximation listed next. The difference is shown in the third column and shows the order to which the calculated frequency is from the desired KAM torus. The difference between the desired and the calculated frequency at each propagation time should be smaller than the difference between the desired to the initial frequency calculation. For example, the Mean Anomaly, *M*, had a consistent error difference on the order of 10^{-6} and was increasing as the propagation continued. The initial Mean Anomaly had a difference from the desired frequency on the order of 10^{-8}. The initial frequency had a smaller difference than the new, calculated frequency meaning the KAM torus was not achieved. These results are similar for the RAAN, Ω, and argument of perigee, ω. The RAAN had an initial difference of 10^{-10} but the error between the desired and the calculated frequency was on the order of 10^{-7}. Finally, ω, had an initial difference of 10^{-9} but the difference between the calculated and the desired was greater at 10^{-7}.

The secular rate values were also used to compare the new KAM torus frequencies and are shown in Table 9 underneath the new KAM torus frequencies. The secular rates were calculated using Equations (57) - (59). The calculated secular rates were within a difference of 10^{-4}. This might be due to the secular drift calculations taking into effect more gravity effects like J_4 than the STK HPOP model integration. The RAAN frequency and the argument of perigee both experienced smaller differences on the order of 10^{-7} and the error was decreasing for the ω term but larger for the Ω terms. The goal here is to also have these difference be lower than the initial vs the desired frequency but this was also not the case.

The following figures (Figure 21 - Figure 26) show the data curve fit graphs for the three KAM torus frequencies, *M*, Ω, and ω along with the residuals. The residuals for the Mean Anomaly, *M*, and the Argument of Perigee, ω, were small and varied between +/- 0.03 radians once again and the node, Ω, were even smaller a 10^{-4}. The errors for the fit graphs were calculated with a level of certainty of 95% in MATLAB meaning there is a 95% chance that the new observation is actually contained within the lower and upper prediction bounds. The confidence bounds determined the amount of error for the fitted coefficients for each frequency while the final frequency calculations in Table 9 are a result of the chosen KAM torus frequency.

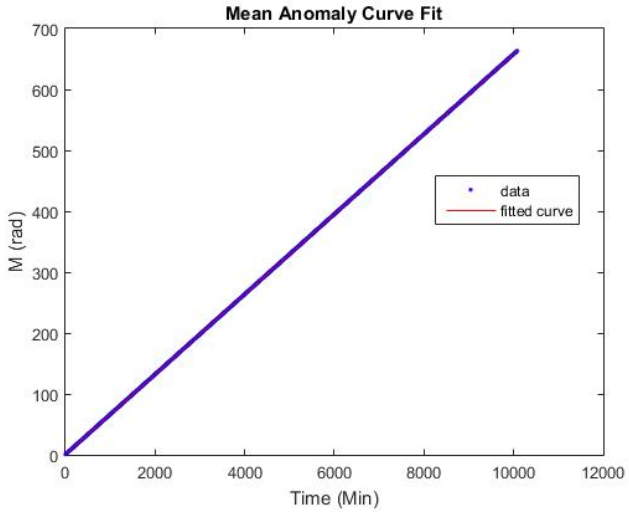

Figure 21: Mean Anomaly Curve Fit after Maneuver

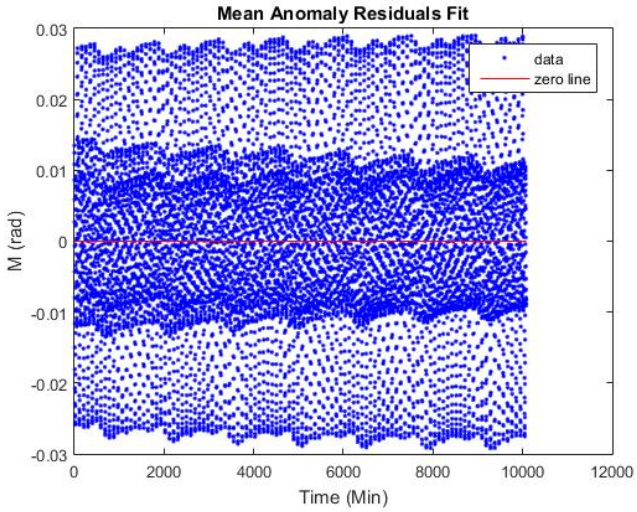

Figure 22: Mean Anomaly Residuals after Maneuver

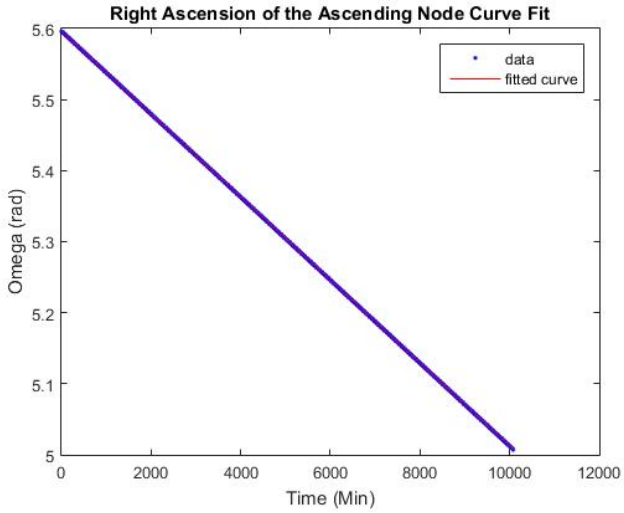

Figure 23: RAAN Curve Fit after Maneuver

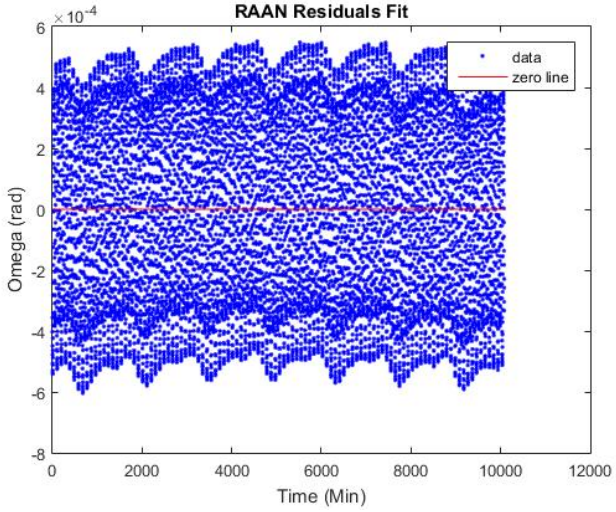

Figure 24: RAAN Residuals after Maneuver

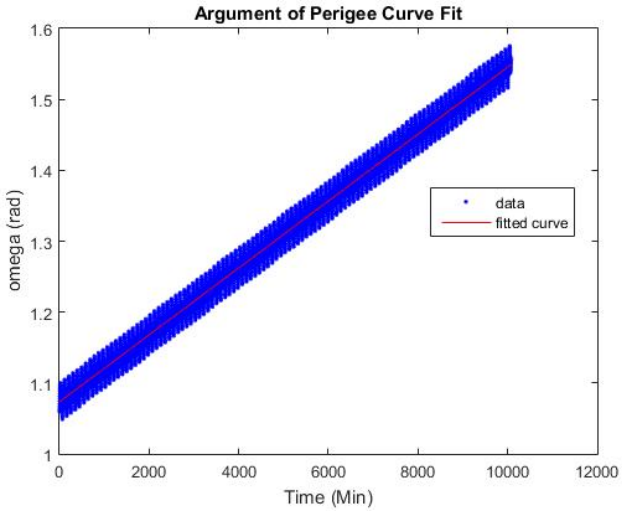

Figure 25: Argument of Perigee Curve Fit after Maneuver

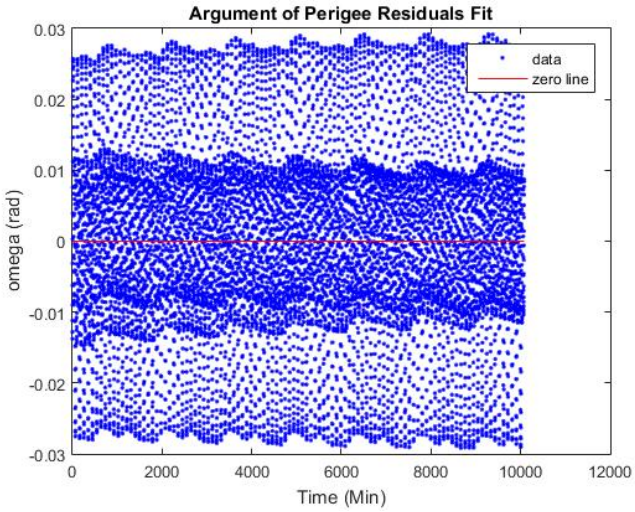

Figure 26: Argument of Perigee Residuals after Maneuver

4.3 Second Test Case (2 week initial propagation time)

The second test case recommended was a two week satellite propagation time in STK to create an ephemeris file that generated the COE of the satellite at every minute of the orbit. The satellite properties used for the second test case can be seen in Table 10**.**. The COE for the

second test case were the same as the first test case and the first satellite but the stop time was 8 Sep 2016 at 16:00 to gather data for a two week propagation time.

Table 10: Orbital Parameters 2nd Test Case

Parameter	Value
Propagation Time	16 days
Semi-major Axis	6928.14 km
Eccentricity	0.03
Inclination	50 deg
Argument of Perigee	30 deg
RAAN	0 deg
True Anomaly	360 deg

4.3.1. Initial Frequency Calculations (Test Case 2)

The data curve fit graphs for the three KAM torus frequencies, M, Ω, and ω can be seen in Figure 12 through Figure 17 along with the residuals. The residuals for the Mean Anomaly, M, and the Argument of Perigee, ω, were similar to Test Case 2 but also increased as the orbit propagated and varied between +/- 0.03 radians. The residuals for RAAN were consistently +0.004 radians and decreasing to -.001 radians by the end of the propagation time.

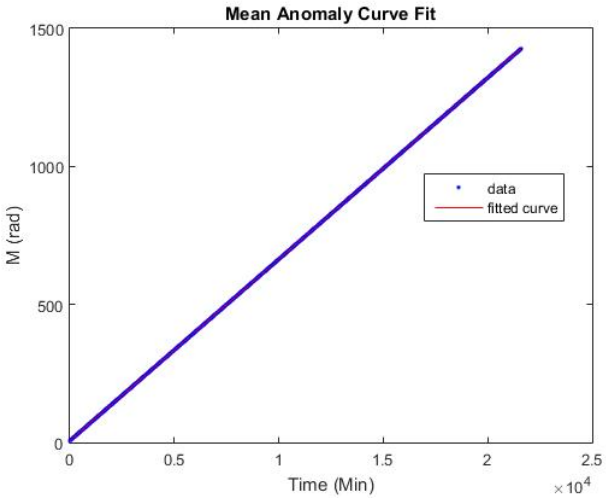

Figure 27: Mean Anomaly Curve Fit (Test 2)

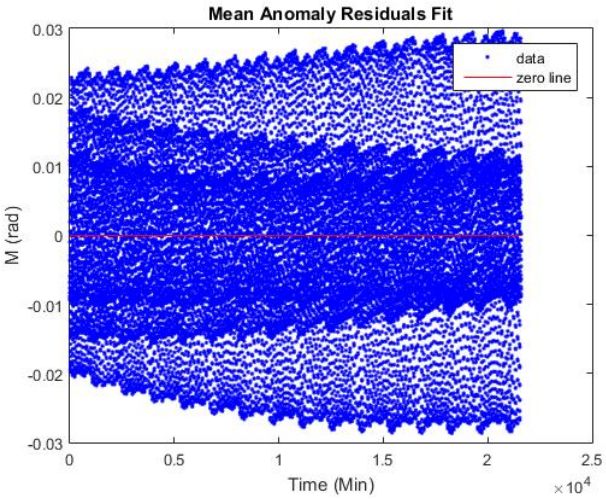

Figure 28: Mean Anomaly Residuals (Test 2)

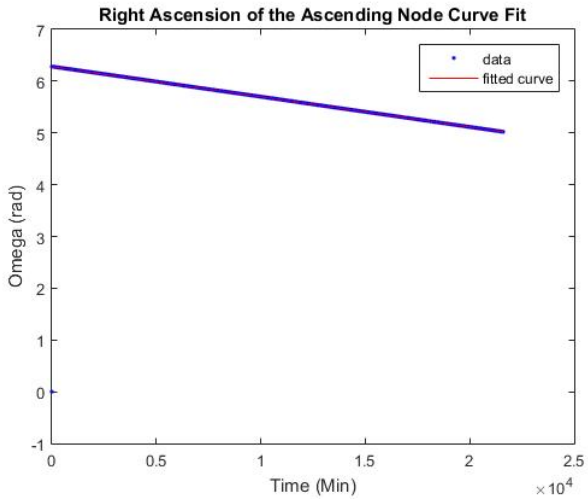

Figure 29: RAAN Curve Fit (Test 2)

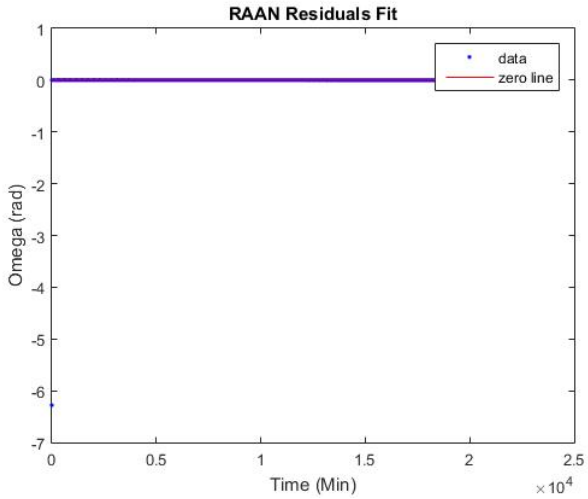

Figure 30: RAAN Residuals (Test 2)

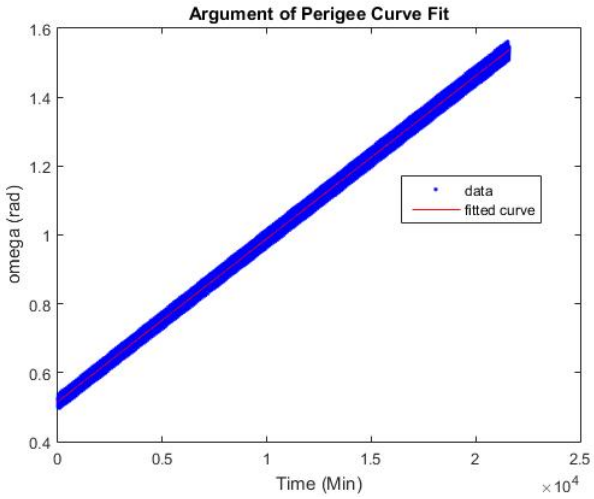

Figure 31: Argument of Perigee Curve Fit (Test 2)

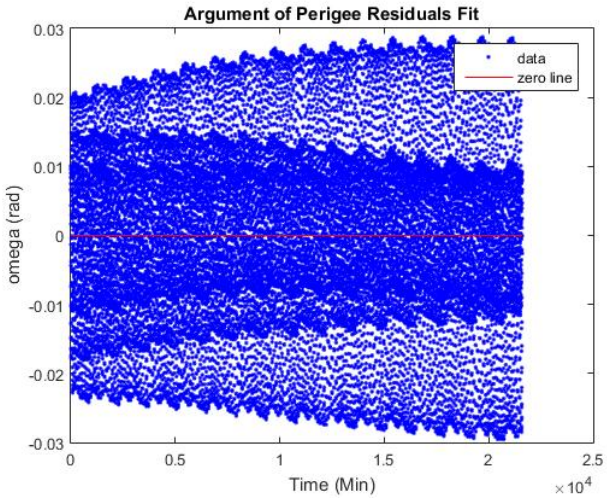

Figure 32: Argument of Perigee Residuals (Test 2)

4.3.2. New KAM torus frequency (Test Case 2)

The KAM torus frequencies were altered from the truth model to the new KAM torus frequencies as shown in Table 11. The new frequencies had a difference of 10^{-6} for the Mean Anomaly, 10^{-6} for the RAAN, and 10^{-11} for the argument of perigee. The differences were chosen based on the first test case results. The new desired frequency used less significant figures and attempted to place the satellite on a KAM torus with a larger frequency change that was on the same value as the difference calculated in Table 9 on the order of 10^{-6}. The argument of perigee was not changed.

Table 11: New KAM Torus Frequencies

Angle	Desired Frequency *(rad/min)*	Initial Frequency *(rad/min)*	Difference
M	0.065800000	0.065745928988109	-5.407101189E-06
Ω	-0.0000582000	-0.000058225621716	-1.6225621719E-06
ω	0.000047296000	0.000047296236572	2.36572E-11

4.3.3. The Two Impulse Maneuver Data

The second impulse maneuver data used the new frequency and attempted to place the satellite on that torus with faster delta-v maneuvers as shown in Table 12.

Table 12: Two Impulse Maneuver Data Test 2

	1st Maneuver	2nd Maneuver
Time (TU)	2 hrs 19 min 21.50 sec	5 hrs 2 min 45.49 sec
$V\hat{\imath}\left(^{km}/_{s}\right)$	8.10958e-03	-1.49544e-01
$V\hat{\jmath}\left(^{km}/_{s}\right)$	6.79026e-01	6.01034e-01
$V\hat{k}\left(^{km}/_{s}\right)$	3.56815e-02	-1.87324e-01

The maneuver cost graph for the second maneuver is shown in Figure 33. The delta-v increased by a factor of three when compared to the first maneuver cost graph in Figure 20.

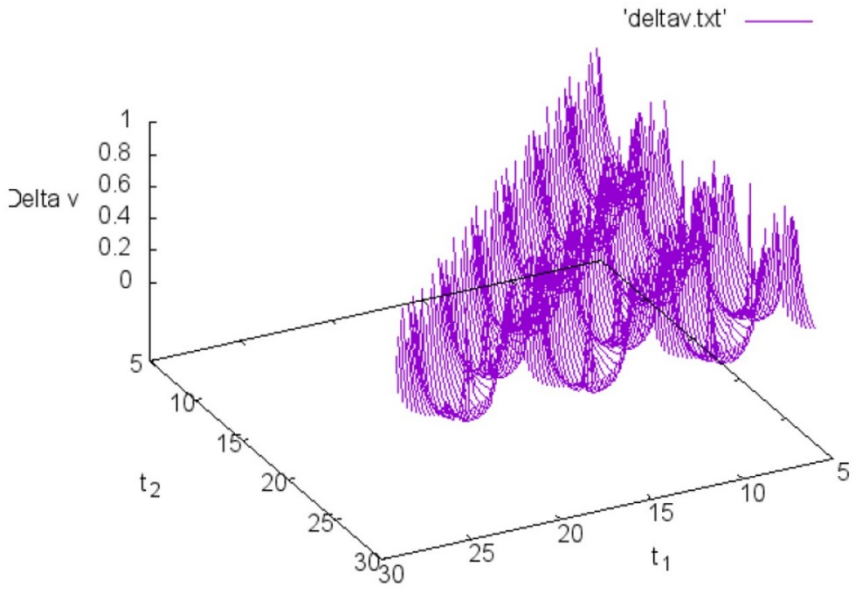

Figure 33: Maneuver Cost Graph Test Case 2 [13]

The new KAM torus frequencies were undefined as the orbit after the first maneuver intersected the Earth at 17 minutes after the first delta-v was implemented. The satellite

trajectory is shown by the red line in Figure 32. The second delta-v maneuver was not implemented as a new position and velocity could not be determined. To implement the second delta-v maneuver, that should have occurred two hours and forty-three minutes after the first delta-v maneuver the satellite needed to maintain a representative orbit trajectory. The delta-v maneuver is believed to be too fast for the orbit and Wiesel's two-impulse maneuver code does not account for Earth intersection when determining the delta-v maneuvers.

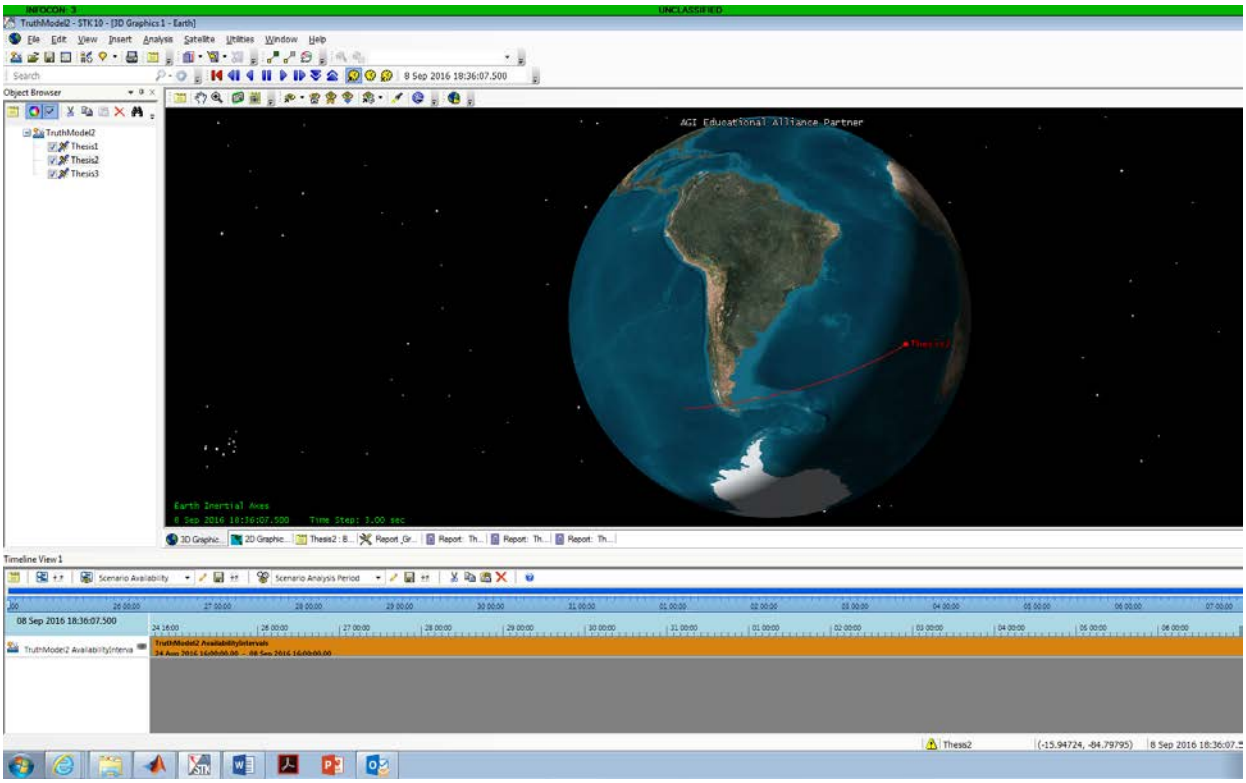

Figure 34: Satellite2 First Maneuver

4.4 Investigative Questions Answered

- Can accurate KAM Torus frequencies be modeled in STK using HPOP and derived from the linear least squares method?

The results in both test cases show using the linear least squares method from the COE produces rough KAM torus frequencies. The HPOP property within STK is very accurate and can create a precise model of the force model environment for almost any satellite [30]. The STK ephemeris data is valuable for KAM torus prediction but a more accurate approach needs to be defined to determine the torus within an orbit. Possibly going back to Craft's approach using Fourier analysis and spectral decomposition to determine the KAM torus frequency would produce a more accurate calculation [26].

- Can a satellite be placed on a desired KAM Torus with two delta-v maneuvers using the COEs?

The results show from the first test case in Table 9 that the differences were on the order of 10^{-6} or greater causing the satellite to lie on a different torus when compared to the initial difference of 10^{-7}. In order for the satellite to lie on the same torus the frequencies need to match with less difference. Perhaps a longer satellite propagation time on both ends of the calculation will aid in creating a more accurate KAM torus frequency set.

The second test case did not yield quantifiable frequencies for the new torus as the satellite's orbit intersected the earth soon after the first delta-v maneuver. The two-impulse maneuver code does not take into account Earth interception when it produces delta-v maneuvers using the 2-body problem and J_2 effects. It is possible the two-impulse maneuver code does not align with the orbital integration accuracy of the STK HPOP force models. Therefore, the orbital insertion rate determined by the two-impulse maneuver code, will not match the STK HPOP orbit causing different KAM torus frequencies.

V. Conclusions and Recommendations

5.1 Chapter Overview

The lasting influence of Kolmogorov, Arnold, and Moser's (KAM) theory on orbital mechanics is yet to be seen. In order to see all of the benefits KAM theory has to offer there needs to be additional development in this field of study. The final chapter summarizes the results of the analysis, conclusions on what the research produced and the impact of what the research means for the KAM torus applications. Recommendations for future work are also presented to help guide the next investigation on the KAM theory and attempt to realize the advantages it has to offer.

5.2 Conclusions of Research

The evidence indicates that this particular scenario of "fixing" a satellite on a desired KAM torus using two delta-v maneuvers is not suitable. The difference for the first test case were on the order of 10^{-7} or greater causing the satellite to lie on a different torus. Even when the orbit was propagated out to three weeks the frequency would not match up to the desired value needed to consider the satellites on the same torus accurately. The second test case attempted to propagate the initial orbit out to two weeks and develop a more accurate KAM torus. The desired torus was different by two significant figures to try to decrease the difference from the first frequency calculations. However, after the first maneuver the satellite orbit intersected the earth and the new frequencies could not be calculated.

The results show that using Systems Tool Kit (STK) and the High Precision Orbit Propagator (HPOP) to calculate KAM torus frequencies can be a reasonable approach when compared to the secular drift rates calculated with an error of less than 0.01 rad. The difference

is due to the secular rates taking into account more gravity effects in J_4. The frequencies calculated using the linear least squares method are a rough estimation and a new method needs to be developed to create more accurate frequencies from the STK model. There is also a possibility that the two-impulse maneuver code does not align with the HPOP force models and will not calculate accurate delta-v maneuvers to place on the exact KAM torus specified.

5.3 Significance of Research

This research has added to the investigation of KAM torus theory by showing the method of inserting into a nearby torus with slightly different momenta, using classical orbital elements, is difficult if not impossible to do with current delta-v maneuvers. If successfully proven this method would make KAM theory available to the wider astrodynamics community with a method that uses a more practical approach. The difficulty seen in the torus calculation process emphasizes the fact that small eccentricity orbits are difficult to model to the desired degree of accuracy with the current KAM torus approaches.

Along with General Hyten's requirement to make satellite more maneuverable the KAM torus theory will enable the Air Force to predict exact satellite position and continue to monitor constellations with more accuracy. This concept could eventually deliver a more practical approach to satellite orbit determination that will save money and keep the satellites within limitations for years to come.

5.4 Recommendations for Future Research

Additional areas of research are needed in the study of KAM theory in order to envision the full effect it has on conservative dynamical systems. First, a KAM torus construction method could be produced and used for autonomous satellites or space debris to more

accurately predict position, velocity and time if used in conjunction with GPS tracking applications. An analysis could be done to determine basis KAM frequencies of specific orbits with different altitudes and inclination combinations. This would show characteristics at different orbits and determine how KAM theory could be applied at different orbits.

Another study could be performed to show how much of the residuals of KAM Torus insertion methods are from air-drag, and how much are due to other perturbation effects that are not easily modeled in STK. This could be done if data was used from real satellites and space-debris at different altitudes. The results could then be compared to derived position vectors from current celestial mechanical methods to show if KAM theory methods are more accurate or not.

Finally, the KAM formation design theory should be investigated. If a spacecraft formation of small satellites was launched and sequenced in a way to place them in orbit together; a KAM torus would be achievable. Similar to Galileo, propagating a satellite out for years to determine a suitable KAM torus might be the next step to making KAM torus a practical approach. Next, using the natural drift of the KAM torus could achieve the desired mission spacecraft formation.

5.5 Summary

First, being fully aware of the limited precision of launch and orbital insertion capabilities, to maneuver onto a specific KAM torus was challenging, if not unfeasible. The research is beneficial to the study of orbital mechanics with the increased competition seen in the Earth orbit environment. A method that increases the prediction of spacecraft position, velocity and time from weeks to months and even years would aid in not only numerous

commercial endeavors but also national security within space. Using previous research from the classical KAM theorem, with the stability of motions in integrable Hamiltonian systems, and the existence of action angle coordinates to confirm KAM frequencies could lead to the long-term prediction needed. KAM torus frequency orbit insertion using two delta-v maneuvers was not practical in this case but this research should encourage the study to continue to find a method feasible that will improve orbit prediction for future generations.

Bibliography

[1] Department of Defense (DoD), "National Security Space Strategy," 2011. [Online]. Available: https://www.defense.gov/News/Special-Reports/National-Security-Space-Strategy.

[2] D. Martin, "The Battle Above," CBS News, 26 April 2015. [Online]. Available: http://www.cbsnews.com/news/rare-look-at-space-command-satellite-defense-60-minutes/. [Accessed 12 12 2016].

[3] D. E. Swenson, Interviewee, *Intermediate Spacraft Dynamics Part 1.* [Interview]. 30 March 2016.

[4] Iridium Communications, "The Global Network: Satellite Constellation," Iridium Everywhere, McClean, Virginia, 2012.

[5] Iridium Satellite LLC, "Orbital Debris Mitigation," Federal Communications Commission, 2000.

[6] Roadpost, "inReach Network & Coverage," 2016. [Online]. Available: http://www.roadpost.ca/inreach_network_coverage.aspx. [Accessed 15 11 2016].

[7] United States Government, "GPS Overview: Space Segement," U.S. Air Force, 9 March 2016. [Online]. Available: http://www.gps.gov/systems/gps/space/. [Accessed 18 August 2016].

[8] D. J. Raquet, Interviewee, *EENG 533 Navigation Using GPS.* [Interview]. 3 February 2016.

[9] GPS.gov, "The Global Positioning System," U.S. Air Force, 26 September 2016. [Online]. Available: http://www.gps.gov/systems/gps/. [Accessed 15 11 2016].

[10] European Space Agency, "GALILEO Fact Sheet," ESA, 3/15/2013.

[11] A. Perez-Cambriles, J. A. Bejar-Romero, D. Aguilar-Taboada and F. Perez-Lopez, "Galileo station keeping strategy," GMV Aerospace & Defense S.A. (www.gmv.com), Spain, 2011.

[12] D. N. Reyes, A. P. Cambriles and J. B. Romero, "GALILEO Station Keeping Strategy," ESA, 2009.

[13] W. Weisel, "Two-Impulse Strategy Program Notes," AFIT, Wright-Patterson AFB, 2017.

[14] C. Hall, Spacecraft Attitude Dynamics and Control, Virginia-Tech, 2011.

[15] D. L. Kunz, MECH 521 Intermediate Dynamics Text, Wright-Patterson AFB: AFIT, 2015.

[16] C. Giesel, "Lesson 1 Dynamics Review Notes," in *MECH 532*, Wright-Patterson AFB, AFIT, 2015.

[17] J. J. Sellers, Understandin Space: An Introduction to Astronautics, New York: The McGraw-hill Companies, Inc., 2000.

[18] W. E. Wiesel, Spaceflight Dynamics, Wright-Patterson AFB: Aphelion Press, 2010.

[19] C. Geisel, Lesson 5: Classical Orbital Elements, Wright-Patterson AFB: AFIT, 2015.

[20] W. E. Wiesel, Modern Astrondynamics, Wright-Patterson AFB: Aphelion Press, 2010.

[21] D. Morin, Introduction to Classical Mechanics, United Kingdom: Cambridge University Press, 2008.

[22] H. Goldstein, Classical Mechanics, San Francisco: Addison Wesley Publishing Company, 1953.

[23] D. L. Chierchia and D. J. N. Mather, "Kolmogorov-Arnold-Moser theory," Scholarpedia, 2010. [Online]. Available: http://www.scholarpedia.org/article/Kolmogorov-Arnold-Moser_theory. [Accessed 28 July 2016].

[24] C. E. Wayne, "An Introduction to KAM Theory," 22 January 2008. [Online]. Available: http://math.bu.edu/people/cew/preprints/introkam.pdf. [Accessed 10 2016].

[25] C. A. Dunk, "Applying KAM Theory to Highly Eccentric Orbits," Wright-Patterson AFB, Dayton, OH, 2014.

[26] C. T. Craft and D. W. Wiesel, "Formation Flight of Earth Satellites on KAM Tori," AAS, Dayton, OH, 2015.

[27] C. G. Frey, "KAM Torus Frequency Generation From Two-Line Element Sets," Wright-Patterson AFB, Dayton, OH, 2011.

[28] R. Abay, "KAM Torus Orbit Prediction From Two Line Element Set," AFIT, Wright-Patterson AFB, 2014.

[29] W. E. Wiesel, "Earth Satellite Orbits As KAM Tori," *The Journal of the Astronautical Sciences,* Vols. 151-162, 2008.

[30] S. T. K. (STK), "High-Precision Orbit Propagator (HPOP)," System Took Kit (STK), Oct 2016. [Online]. Available: http://help.agi.com/stk/index.htm#hpop/hpop.htm. [Accessed Nov 2016].

[31] J. Poschel, "A Lecture on the Classical KAM Theorem," in *Mathematical Aspects of Classical and Celestial Mechanics,* Third ed., Berlin, Springer, 2006, pp. 707-732.

[32] V. I. Arnol'd and A. Givental, Collected Works, Dordrecht: Springer, 2009.

[33] W. E. Wiesel, Modern Orbit Determination, Wright-Patterson AFB: Aphelion Press, 2010.

REPORT DOCUMENTATION PAGE

Form Approved
OMB No. 074-0188

The public reporting burden for this collection of information is estimated to average 1 hour per response, including the time for reviewing instructions, searching existing data sources, gathering and maintaining the data needed, and completing and reviewing the collection of information. Send comments regarding this burden estimate or any other aspect of the collection of information, including suggestions for reducing this burden to Department of Defense, Washington Headquarters Services, Directorate for Information Operations and Reports (0704-0188), 1215 Jefferson Davis Highway, Suite 1204, Arlington, VA 22202-4302. Respondents should be aware that notwithstanding any other provision of law, no person shall be subject to any penalty for failing to comply with a collection of information if it does not display a currently valid OMB control number.
PLEASE DO NOT RETURN YOUR FORM TO THE ABOVE ADDRESS.

1. REPORT DATE *(DD-MM-YYYY)*	2. REPORT TYPE	3. DATES COVERED *(From – To)*
23-Mar-2017	Master's Thesis	Mar 2016 – Mar 2017

4. TITLE AND SUBTITLE
FORMATION FLIGHT OF EARTH SATELLITES ON KAM TORUS USING CLASSICAL ORBITAL ELEMENTS

5a. CONTRACT NUMBER

5b. GRANT NUMBER

5c. PROGRAM ELEMENT NUMBER

6. AUTHOR(S)
Reabe, Marissa C, Capt,USAF

5d. PROJECT NUMBER
NA

5e. TASK NUMBER

5f. WORK UNIT NUMBER

7. PERFORMING ORGANIZATION NAMES(S) AND ADDRESS(S)
Air Force Institute of Technology
Graduate School of Engineering and Management (AFIT/EN)
2950 Hobson Way, Building 640
WPAFB OH 45433-8865

8. PERFORMING ORGANIZATION REPORT NUMBER
AFIT-ENY-MS-17-M-285

9. SPONSORING/MONITORING AGENCY NAME(S) AND ADDRESS(ES)
Intentionally Left Blank

10. SPONSOR/MONITOR'S ACRONYM(S)

11. SPONSOR/MONITOR'S REPORT NUMBER(S)

12. DISTRIBUTION/AVAILABILITY STATEMENT

DISTRIBUTION STATEMENT A.APPROVED FOR PUBLIC RELEASE; DISTRIBUTION UNLIMITED.

13. SUPPLEMENTARY NOTES
This material is declared a work of the U.S. Government and is not subject to copyright protection in the United States.

14. ABSTRACT
This research uses the KAM theory that has been refined by Wiesel to show that Earth-satellites dynamics can be represented by an integrable Hamiltonian system with a small perturbation, like Earth's geopotential. The satellite will follow a torus in phase space and remain on that KAM torus for all time unless acted on by a non-conservative force. A torus frequency was calculated, in this research, using a truth model in System Tool Kit (STK) and the High Precision Orbit Propagator (HPOP) to develop an accurate ephemeris file listing the Classical Orbital Elements (COEs). The frequencies found from the truth model were then used to calculate two delta-v maneuvers to insert a satellite onto a desired KAM torus at a specified position and time. Ultimately, this method could be a practical approach to the wider astronautics community to calculate a more accurate satellite position and time over longer periods when compared to current orbital mechanics methods. The results indicated that this particular scenario of "fixing" a satellite on a desired KAM torus using two delta-v maneuvers is not suitable. The residuals for the first test case were on the order of 10^{-7} or greater causing the satellite to lie on a different torus.

15. SUBJECT TERMS
KAM, Torus, Tori, satellite, formation, COE, STK, HPOP, constellation

16. SECURITY CLASSIFICATION OF:			17. LIMITATION OF ABSTRACT	18. NUMBER OF PAGES	19a. NAME OF RESPONSIBLE PERSON
a. REPORT	b. ABSTRACT	c. THIS PAGE			William E. Wiesel, PhD
U	U	U	UU	92	19b. TELEPHONE NUMBER *(Include area code)* (937) 255-3636, x 3329 (William.wiesel@afit.edu)